coming paper.[13] It is based on a symmetric ion with two equivalent Ru centers and does include explicit consideration of the electronic structure of the bridge and of spin–orbit coupling. A straightforward interpretation of the near-infrared spectra containing more than one absorption band is not possible for the two ions within the framework of either the Hush model or the Hückel MO approach. Both descriptions allow for only one low-energy transition, the so-called "intervalence transition".

Acknowledgment. We thank Dr. H. Wagner, CIBA Geigy, Basel, for the elemental analyses. This work was supported by the Swiss National Science Foundation (Grant No. 2.209-0.81).

Supplementary Material Available: Listings of structure factors, thermal parameters, hydrogen positions, and bond lengths and angles for the anions of I and II and stereoviews of the unit cell of I and II (70 pages). Ordering information is given on any current masthead page.

(13) Joss, S.; Fürholz, U.; Hasselbach, K. M.; Bürgi, H. B.; Wordel, R.; Wagner, F. E.; Ludi, A., to be submitted for publication.

Contribution from the Department of Chemistry, University of California, Berkeley, California 94720

Ferric Ion Sequestering Agents. 13. Synthesis, Structures, and Thermodynamics of Complexation of Cobalt(III) and Iron(III) Tris Complexes of Several Chelating Hydroxypyridinones[1]

ROBERT C. SCARROW, PAUL E. RILEY, KAMAL ABU-DARI, DAVID L. WHITE, and KENNETH N. RAYMOND*

Received July 10, 1984

Metal complexes of bidentate hydroxypyridinone ligands have been prepared and characterized. The pseudooctahedral Co(III) and Fe(III) tris complexes of 1-hydroxy-2(1*H*)-pyridinonate (1,2-opo) and the Fe(III) tris complex of 3-hydroxy-2(1*H*)-pyridinonate (3,2-opo) have been characterized by single-crystal X-ray diffraction. Variable-temperature NMR shows the cobalt complex is conformationally labile in $CDCl_3$. Determination of the formation constants of the Fe(III) complexes of several chelating hydroxypyridinone monoanions by spectrophotometric titration demonstrates that these ligands have chelation affinities for Fe(III) that are intermediate between those of monoanionic hydroxamate and dianionic catecholate species. The relatively strong acidities of the hydroxypyridinones (pK_a's = 5–9) enable them to chelate ferric ion more effectively than catechol or hydroxamates in neutral or acidic solutions. The crystal structures of all the metal complexes are disordered with respect to the location of the nitrogen in the bidentate opo ligands. Two structurally similar forms of dark green Co(1,2-opo)$_3$ crystals were observed; one is $P2_1/n$ with a = 9.702 (2) Å, b = 9.516 (2) Å, c = 17.146 (3) Å, β = 103.41 (1)°, and Z = 4, and the other is $C2/c$ with a = 15.142 (2) Å, b = 9.507 (1) Å, c = 10.845 (1) Å, β = 96.00 (1)°, and Z = 4. Full-matrix least-squares refinement (on $|F|$) using 2589 and 882 reflections with $F_o^2 > 3\sigma(F_o^2)$ has converged with R = 0.063 and 0.024 and R_w = 0.071 and 0.031, respectively. Crystals of the tris complexes of Fe(III) with the 1,2-opo and 3,2-opo isomers form in space group $R\bar{3}c$. The Fe(1,2-opo)$_3$ complex crystallizes as yellow-orange parellelepipeds with $a = b$ = 9.634 (1) Å, c = 31.290 (5) Å (hexagonal setting), and Z = 6. Refinement using 556 reflections with $F_o^2 > 3\sigma(F_o^2)$ converged to R = 0.021 and R_w = 0.035. The Fe(3,2-opo)$_3$ complex forms as orange plates with $a = b$ = 9.782 (1) Å, c = 29.615 (3) Å, and Z = 6. Refinement using 629 observations with $F_o^2 > 3\sigma(F_o^2)$ converged to R = 0.024 and R_w = 0.035. Yellow-white needles of the uncomplexed molecule *N,N*-dimethyl-1-hydroxy-2-(1*H*)-pyridinone-6-carboxamide are of space group $P2_1/n$ with a = 18.803 (2) Å, b = 9.274 (1) Å, c = 4.969 (1) Å, β = 96.10 (1)°, and Z = 4. Refinement using 1183 reflections with $F_o^2 > 3\sigma(F_o^2)$ converged to R = 0.041 and R_w = 0.061.

Introduction

Siderophores are low-molecular weight compounds manufactured by microorganisms to facilitate the uptake of Fe(III), the concentration of which ($\sim 10^{-18}$ M) is severely limited by the extremely low solubility of ferric hydroxide ($K_{sp} \simeq 10^{-38}$) at physiological pH.[2] The most common functional groups of the siderophores are the hydroxamate (**1**) and catecholate (**2**) moieties,

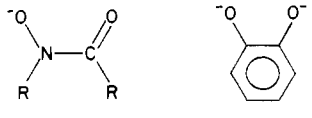

1 2

which act as strong bidentate chelating agents for Fe(III). In our efforts to design more effective sequestering agents for use in the treatment of human iron toxicity,[3] we and others have mimicked the efficient naturally occurring iron sequestering agents (such as enterobactin, the ferrichromes, and ferrioxamines) by incorporating catecholate and hydroxamate functionalities into synthetic macrochelating ligands.[4-6] These synthetic iron chelators have also proven useful in studies of the mechanisms of microbial iron uptake[7,8] and of iron removal from mammalian iron transport proteins.[4,9]

Recently we have begun investigation of other bidentate functional groups for possible use in siderophore-type complexing agents. This report describes the iron and cobalt complexes of several hydroxypyridinones ("Hopo's") in which the hydroxy group is ortho to the ketone functionality. The three unsubstituted chelating hydroxypyridinones and their abbreviations are shown in Figure 1. The deprotonated ligands will be abbreviated as "opo's": i.e., 1,2-opo$^-$, 3,2-opo$^-$, 3,4-opo$^-$.

(1) Previous paper in this series: Kappel, M. J.; Pecoraro, V. L.; Raymond, K. N. *Inorg. Chem.*, in press.
(2) Smith, R. M.; Martell, A. E. "Critical Stability Constants"; Plenum Press: New York, 1974–1977; Vol. 1–4.
(3) Martell, A. E., Anderson, W. F., Badman, D. G., Eds. "Development of Iron Chelators for Clinical Use"; Elsevier/North-Holland: 1981.
(4) Raymond, K. N.; Chung, T. D. Y.; Pecoraro, V. L.; Carrano, C. J. "The Biochemistry and Physiology of Iron"; Saltman, P., Hegenauer, J., Eds.; Elsevier Biomedical: New York, 1982; pp 649–662.
(5) Raymond, K. N.; Tufano, T. P. "The Biological Chemistry of Iron"; Dunford, H. B., Dolphin, D., Raymond, K. N., Seiker, L., Eds.; D. Reidel: Dordrecht, Holland, 1982; pp 85–105.
(6) Raymond, K. N.; Pecoraro, V. L.; Weitl, F. L. "Development of Iron Chelators for Clinical Use"; Martell, A. E., Anderson, W. F., Badman, D. G. , Eds.; Elsevier/North-Holland, 1981: pp 165–187.
(7) Heidinger, S.; Braun, V.; Pecoraro, V. L.; Raymond, K. N. *J. Bacteriol.* **1983**, *153*, 109–115.
(8) Raymond, K. N.; Müller, G.; Matzanke, B. F. *Top. Curr. Chem.* **1984**, *123*, 50–102.
(9) Rodgers, S. J.; Raymond, K. N. *J. Med. Chem.* **1983**, *26*, 439–442.

0020-1669/85/1324-0954$01.50/0

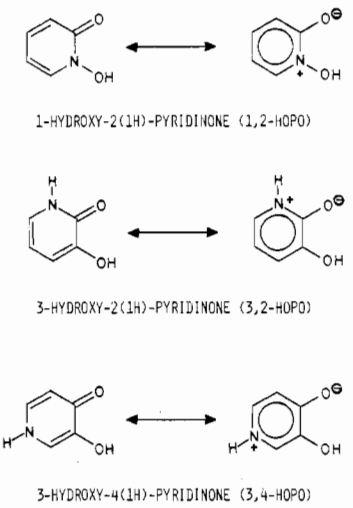

Figure 1. The simple chelating hydroxypyridinones and their abbreviations.

Such molecules have features in common with both catechols and hydroxamic acids. All of these ligands form five-membered chelate rings in which the metal ion is bound by two oxygen atoms. Like hydroxamic acids, the hydroxypyridinones are monoprotic acids that bind to metals by an oxyanion and an oxo group. In fact, 1-hydroxy-2(1*H*)-pyridinone (1,2-Hopo) may be viewed as a cyclic hydroxamic acid. But the deprotonated hydroxypyridinones have a zwitterionic aromatic resonance form (Figure 1) which is isoelectronic with the catecholate dianion. There is a substantial amount of delocalization in the bonding of the catecholate anion to Fe(III), which contributes to the great stability of these complexes.[10] This is also possible for the iron–hydroxypyridinone complexes.

In this paper we report the syntheses and crystal structures of the tris complexes of 1-hydroxy-2(1*H*)-pyridinonate with Co(III) and Fe(III), the synthesis and structure of the tris(3-hydroxy-2-(1*H*)-pyridinonate) complex of Fe(III), and the preparation and crystal structure of the electronegative ligand *N*,*N*-dimethyl-1-hydroxy-2(1*H*)-pyridinone-6-carboxamide (abbreviated 1,2-Hopo-6-Y), as well as the preparation and characterization of the tris complex of the anion of this ligand with Fe(III).[11] To aid in our evaluation of the relative affinity of these ligands for iron, we have investigated the thermodynamics of the binding of Fe(III) by the three simple hydroxypyridinone isomers as well as the dimethylcarboxamide derivative.

The binding of actinide(IV) ions by ligands such as hydroxamates and catecholates closely parallels that with high-spin Fe(III). This has formed the basis for the design of actinide(IV)-specific macrochelate sequestering agents.[12,13] We have studied related actinide(IV) (and analogous metal(IV) cation) complexes with catechol,[14-16] thiohydroxamate,[17] and 1,2-opo.[18]

Experimental Section

Materials. The ligands 1-hydroxy-2(1*H*)- and 3-hydroxy-2(1*H*)-pyridinone were purchased from Aldrich Chemical Co., sodium cobaltinitrite ($Na_3[Co(NO_2)_6]$) was obtained from Allied Chemical Corp., and ferric nitrate nonahydrate and potassium nitrate were purchased from Mallinckrodt Chemical Co. Mimosine ((*S*)-α-amino-3-hydroxy-4-oxo-1(4*H*)-pyridinepropanoic acid), 99%, was purchased from Sigma Chemical Co. and used as supplied. Reagent grade ferric and sodium perchlorates were purchased from G. F. Smith Chemical Co. Solvents were analytical grade and used as supplied.

For titration studies 1-hydroxy-2(1*H*)- and 3-hydroxy-2(1*H*)-pyridinone were sublimed at 100 (30 mtorr) and 150 °C (<1 mtorr), respectively. Disodium EDTA (Sigma 99%) was purified by recrystallization from 95% ethanol following the procedure of Blaedel and Knight.[19] Ferric nitrate and ferric perchlorate stock solutions were prepared and standardized by a method described previously[20] or by EDTA titrations using variamine B blue as the indicator.[21] Metal impurities in potassium nitrate (Mallinckrodt AR) were removed by extraction twice with 3:1 benzene–carbon tetrachloride containing 8-hydroxyquinoline, followed by recrystallization from hot water.

Instruments. Infrared and mass spectra were obtained with Perkin-Elmer Model 283 and AEI MS-12 instruments, respectively. The 250-MHz variable-temperature NMR and 300-MHz NMR of $Co(1,2\text{-opo})_3$ were studied on Fourier transform instruments employing Nicolet software. All other NMR spectra employed a 90-MHz JEOL Model FX-900 Fourier transform spectrometer. Routine spectral characterizations are reported in the supplementary material.

Magnetic susceptibility measurements were carried out on powdered samples in calibrated aluminum containers between 5 and 300 K on a SHE 905 SQUID magnetometer.

Elemental analyses were performed by the UC Berkeley Microanalytical Laboratory.

Syntheses. Tris[1-hydroxy-2(1*H*)-pyridinonato]cobalt(III) (3; Co(1,2-opo)$_3$). To an ethanol solution (10 mL) of 1-hydroxy-2(1*H*)-pyridinone (1.11 g, 10 mmol) was added a degassed aqueous NaOH solution (1.0 M, 10 mL) followed by a degassed aqueous solution of $Na_3[Co(NO_2)_6]$ (1.35 g, 3.30 mmol). The reaction, which began immediately as indicated by an instantaneous appearance of a green precipitate, was accelerated by heating the solution to 80 °C for several hours. The green precipitate was filtered, washed with water to remove the sodium salts, and dried in vacuo over P_2O_5. Slow evaporation of a chloroform–ethanol solution (or a chloroform–heptane solution) yielded dark green irregular blocks of **3a**. These rapidly decompose to a grayish violet solid at 237 °C.

Recrystallization from 2:1 CH_2Cl_2–MeOH gave dark green parellelepipeds **3B**. Anal. Calcd for $Co(C_5H_4NO_2)_3$: C, 46.28; H, 3.10; N, 10.79. Found: C, 45.47; H, 3.33; N, 10.58.

An alternate synthesis of $Co(1,2\text{-opo})_3$ from $Co(OAc)_2{\cdot}4H_2O$ is in the literature.[22]

Tris[1-hydroxy-2(1*H*)-pyridinonato]iron(III) (4; Fe(1,2-opo)$_3$). This complex was prepared by the same procedure as **3**, with $Fe(NO_3)_3{\cdot}9H_2O$ (4.04 g, 10.0 mmol) instead of the Co(III) salt, under an inert atmosphere. Upon addition of the Fe(III) salt, a yellow-orange precipitate formed, which was filtered, washed with water, and dried over P_2O_5. Recrystallization of this material from a chloroform–ethanol solution afforded well-formed yellow-orange parallelepipeds of **4**. These decompose to a brown solid above 250 °C. Anal. Calcd for $Fe(C_5H_4NO_2)_3$: C, 46.66; H, 3.13; N, 10.88. Found: C, 46.71; H, 3.28; N, 10.76.

Tris[3-hydroxy-2(1*H*)-pyridinonato]iron(III) (5; Fe(3,2-opo)$_3$). This complex was prepared under an oxygen-free inert atmosphere via Schlenk-line techniques. A stirred oxygen-free aqueous solution (10 mL) of NaOH (2.4 g) was treated with 3-hydroxy-2(1*H*)-pyridinone (3.33 g, 30.0 mmol) and a filtered, oxygen-free solution (20 mL) of $Fe(NO_3)_3{\cdot}9H_2O$ (0.04 g, 10.0 mmol). The mixture was heated to ~80 °C with stirring and then filtered while hot. Slow cooling of the filtrate yielded purple crystals of **5**, mp >260 °C.

Magnetic susceptibility (10 kG):[23] μ_{eff}(300 K) = 5.84; Curie–Weiss parameters C = 4.327 (5),[24] Θ = −1.20 (18) K, μ_{av} = 5.882 (3). Anal. Calcd for $Fe(C_5H_4NO_2)_3{\cdot}H_2O$: C, 44.58; H, 3.49; N, 10.40. Found: C, 44.18; H, 3.33; N, 10.44.

(10) Gordon, D. J.; Fenske, R. F. *Inorg. Chem.* **1982**, *21*, 2916–2923.
(11) Attempts to obtain useful single crystals of this complex have so far been unsuccessful.
(12) Raymond, K. N.; Freeman, G. E.; Kappel, M. J. *Inorg. Chim. Acta* **1984**, *94*, 193–204.
(13) Raymond, K. N.; Kappel, M. J.; Pecoraro, V. L.; Harris, W. R.; Carrano, C. J.; Weitl, F. L.; Durbin, P. W. "Actinides in Perspective"; Edelstein, N. M., Ed.; Pergamon Press: New York, 1982; pp 491–507.
(14) Freeman, G. E.; Raymond, K. N., submitted for publication to *Inorg. Chem.*
(15) Sofen, S. R.; Cooper, S. R.; Raymond, K. N. *Inorg. Chem.* **1979**, *18*, 1611–1615.
(16) Sofen, S. R.; Abu-Dari, K.; Freyberg, D. P.; Raymond, K. N. *J. Am. Chem. Soc.* **1978**, *100*, 7882–7887.
(17) Abu-Dari, K.; Raymond, K. N. *Inorg. Chem.* **1982**, *21*, 1676–1679.
(18) Riley, P. E.; Abu-Dari, K.; Raymond, K. N. *Inorg. Chem.* **1983**, *22*, 3940–3944.
(19) Blaedel, W. J.; Knight, H. T. *Anal. Chem.* **1954**, *26*, 741–743.
(20) Harris, W. R.; Raymond, K. N. *J. Am. Chem. Soc.* **1979**, *101*, 6534–6541.
(21) Vogel, A. I. "A Textbook of Quantitative Inorganic Analysis", 3rd ed.; Longmans, Green and Co.: London, 1961; p 444.
(22) Hubbard, D.; Eaton, G. R.; Eaton, S. S. *Inorg. Nucl. Chem. Lett.* **1979**, *15*, 255–258.
(23) No perceptible field dependence of χ_M was noted between 2 and 40 kG. Corrections for diamagnetism were -1.82×10^{-4} and -2.35×10^{-4} emu/mol for $Fe(3,2\text{-opo})_3{\cdot}H_2O$ and $Fe(1,2\text{-opo-6-Y})_3{\cdot}0.5H_2O$, respectively (see: Mulay, L. N.; Boudreaux, E. A. "Theory and Application of Molecular Diamagnetism"; Wiley: New York, 1976).
(24) The esd in the least significant digit is given in parentheses.

Table I. Crystallographic Summary[24]

	$Co(1,2\text{-opo})_3$ (3a)	$Co(1,2\text{-opo})_3$ (3b)	$Fe(1,2\text{-opo})_3$ (4)	$Fe(3,2\text{-opo})_3$ (5)	1,2-Hopo-6-Y (10)
a, Å	9.702 (2)	15.142 (2)	9.634 (1)	9.782 (1)	18.803 (2)
b, Å	9.516 (2)	9.507 (1)	a	a	9.274 (1)
c, Å	17.146 (3)	10.845 (1)	31.290 (5)	29.615 (3)	4.969 (1)
β, deg	103.41 (1)	96.00 (1)			96.10 (1)
V, Å^3	1539.8 (9)	1552.5 (3)	2515.1 (9)	2454.1 (8)	861.6 (4)
2θ range for cell constants, deg	27.8–35.7	22.0–32.0	28.1–29.4	28.0–30.0	17.7–21.9
d_{measd}, g cm^{-3}	1.69 (3)[a]	1.67 (1)[c]	1.55 (4)[e]	1.60 (4)[e]	1.42 (4)[i]
d_{calcd}, g cm^{-3}	1.68	1.66	1.53	1.57	1.40
mol formula	$C_{15}H_{12}CoN_3O_6$	$C_{15}H_{12}CoN_3O_6$	$C_{15}H_{12}FeN_3O_6$	$C_{15}H_{12}FeN_3O_6$	$C_8H_{10}N_2O_3$
fw	389.21	389.21	386.13	386.13	182.18
Z	4	4	6	6	4
cryst syst	monoclinic	monoclinic	trigonal (hexagonal axes)	trigonal (hexagonal axes)	monoclinic
space group based on diffracn sym	$P2_1/n$[b] (No. 14)	Cc (No. 9) or $C2/c$ (No. 15)	$R3c$ (No. 161) or $R\bar{3}c$ (No. 167)	$R3c$ (No. 161) or $R\bar{3}c$ (No. 167)	$P2_1/n$[b] (No. 14)
F(000), e	792	792	1182	1182	384
p	0.04	0.02	0.03	0.03	0.035
check reflcns	small random variations in intens during the 116, 29, 24, 74, and 28 h of data collecn for 3a, 3b, 4, 5, and 10, respectively; hence no decay correcns were applied to these data sets				
2θ range for data collecn, deg	2.8–70.0	2.0–45.0	3.0–55.0	3.0–64.0	3.0–50.0
unique reflcns measd	5441	1019[d]	759[f]	938[f]	1508
data cryst dimens, mm	0.18 × 0.18 × 0.50	0.13 × 0.21 × 0.21	0.23 × 0.24 × 0.26	0.10 × 0.24 × 0.25	0.23 × 0.24 × 0.41
abs coeff, μ(Mo Kα), cm^{-1}	12.02	11.39	9.32	9.63[h]	1.18
transmission factor range, %	78.2–82.4	77.6–86.6	[g]	81.8–93.3	[g]

[a] Flotation in a mixture of 1,1-dichloroethane and 1,2-dibromoethane. [b] An alternative setting of space group $P2_1/c$ with equivalent positions $\pm(x, y, z)$, $\pm(1/2 - x, 1/2 + y, 1/2 - z)$. [c] Flotation in a mixture of 1,2-dichloroethane and 1,1-dibromoethane. [d] The equivalent (in $C2/c$) hkl and $\bar{h}k\bar{l}$ reflections were measured and averaged.[28] [e] Flotation in a mixture of carbon tetrachloride and 2-bromopropane. [f] The two equivalent sets of reflections hkl and $kh\bar{l}$ of Laue symmetry class $\bar{3}m$ were collected and then averaged.[28] [g] Examination of four reflections with $\chi \simeq 90°$ at regular intervals ($\Delta 2\theta = 5$–$10°$) throughout the limits of data collection by the ψ-scan technique showed an average variation in normalized transmission factors of 0.95–1.00; hence a correction for absorption was not applied to these data. [h] Calculated with the assumption of one water of hydration, which was subsequently not located. [i] Flotation in a mixture of bromoform and 2-bromopropane.

The water indicated by the analysis could be removed in vacuo at 140 °C overnight (2.9% weight loss vs. 4.5% calculated). Anal. Calcd for $Fe(C_5H_4NO_2)_3$: C, 46.66; H, 3.13; N, 10.88. Found: C, 45.88; H, 2.97; N, 10.68.

2-Bromopyridine-6-carboxylic Acid 1-Oxide (7). A 9.7-g (0.048-mol) portion of 6-bromopyridine-2-carboxylic acid (**6**)[25] was added to a solution of 125 mL of CF_3CO_2H and 18 mL of 30% H_2O_2 and heated to 80 °C for 6.5 h. The reaction mixture was concentrated to ca. 25 mL by rotary evaporation and then added to 1 L of water. The product immediately precipitated as a finely divided, white crystalline solid. It was isolated by filtration, washed with water, and dried in vacuo. This yielded 10.2 g (97%) of product, mp 180 °C dec. Anal. Calcd for $C_6H_4BrNO_3$: C, 33.05; H, 1.85; Br, 36.65; N, 6.43. Found: C, 33.30; H, 1.88; Br. 36.37; N, 6.52.

1-Hydroxy-2(1*H*)-pyridinone-6-carboxylic Acid (8). A 10.1-g (0.046 mol) portion of **7** was dissolved in 175 mL of a 10% aqueous KOH solution, and the resulting solution was maintained at 80 °C overnight and then cooled in an ice bath and treated with 85 mL of concentrated HCl. The white suspended solid was isolated by filtration, washed with dilute HCl followed by three 15-mL portions of water, and then dried in vacuo to yield 6.21 g (86.4%) of 8, mp 216 °C dec. Anal. Calcd for $C_6H_5NO_4$: C, 46.45; H, 3.25; N, 9.03. Found: C, 46.29; H, 3.26; N, 8.96.

Poly[1-hydroxy-2(1*H*)-pyridinone-6-carboxylate] (9). A suspension of 0.5 g (3.2 mmol) of **8** in 10 mL of dry THF was treated with 10 mL of $SOCl_2$. A slightly exothermic reaction was observed upon mixing, and some foaming was noted after the reaction mixture had been heated to 100 °C. After a 4-h reflux period no starting material remained and volatile components of the reaction mixture were removed by bulb-to-bulb distillation. The resulting brownish yellow residue was suspended in dry acetone, filtered, and washed with additional acetone. Drying in vacuo at 25 °C gave 0.41 g (93%) of pale yellow, free-flowing powder. It was identified as the polymeric (or oligomeric) ester on the basis of its insolubility in most organic solvents, negative Beilstein test,[26] and spectroscopic properties. Anal. Calcd for $C_6H_3NO_3$: C, 52.56; H, 2.21; N, 10.22. Found: C, 49.46; H, 2.24; N, 9.36.

***N*,*N*-Dimethyl-1-hydroxy-2(1*H*)-pyridinone-6-carboxamide (10; 1,2-Hopo-6-Y).** Dimethylamine gas was bubbled into a suspension of 0.90 g (6.7 mmol) of **9** in 15 mL of THF. A mildly exothermic reaction ensued, and the solid dissolved within a few minutes. After the mixture was stirred for 30 min at 25 °C with excess dimethylamine, volatile components of the reaction mixture were removed on a rotary evaporator. The residue was dissolved in 5 mL of water and applied to a 1 cm i.d. × 20 cm column of AG-50X-8 ion-exchange resin in the H^+ form. Elution with water gave a yellow, acidic fraction that gave an intense red color when treated with Fe^{3+}. Removal of water on a rotary evaporator gave 0.77 g (64%) of pale yellow, crystalline **10**, mp 165–167 °C.

An analytically pure sample, mp 167.5–168 °C, was obtained by recrystallization from acetone. Anal. Calcd for $C_8H_{10}N_2O_3$: C, 52.74; H, 5.53; N, 15.38. Found: C, 52.62; H, 5.61; N, 15.16.

The reactions with compounds **6**–**10** are summarized in Scheme I.

Tris[*N*,*N*-dimethyl-1-hydroxy-2(1*H*)-pyridinone-6-carboxamidato]-iron(III) (11). A solution of 0.177 g (0.438 mmol) of $Fe(NO_3)_3 \cdot 9H_2O$ in 2 mL of water was added to 0.240 g (1.32 mmol) of ligand **10** that had been dissolved in 5 mL of water. The resulting acidic orange-red solution was neutralized with an aqueous NaOH solution. The orange-red product was extracted into chloroform. Evaporation of the solvent yielded 0.232 g (53.0%) of amorphous residue, which was recrystallized from a methylene chloride–ethanol mixture.

Magnetic susceptibility (5 and 40 kG):[23] μ_{eff}(300 K) = 5.86; Curie–Weiss parameters C = 4.302 (3),[24] Θ = −0.39 (13) K, μ_{av} = 5.891 (2). Anal. Calcd for $C_{24}H_{27}N_6O_9Fe \cdot 0.5H_2O$: C, 47.38; H, 4.64; N, 13.82. Found: C, 47.57, 47.69; H, 4.76, 4.53; N, 13.74, 13.81.

3-Hydroxy-4(1*H*)-pyridinone (3,4-Hopo). This was produced from mimosine by the method of Hart et al.[27] The product was sublimed at 150–165 °C and ca. 0.5 mtorr to yield a slightly greenish but analytically pure powder. Recrystallization from 95% ethanol yielded white crystals, which were used in all titrations. Anal. Calcd for $C_5H_5NO_2$: C, 54.06; H, 4.54; N, 12.61. Found: C, 54.15; H, 4.52; N, 12.64.

X-ray Crystallography. Satisfactory single crystals of **3a**, **3b**, **4**, and **5** were obtained by the methods cited above, while a suitable crystal of **10** was obtained from a large needle by cutting along cleavage planes normal to the (100) and (101) planes. Crystals of **3a**, **4**, and **5** were wedged into thin-walled glass capillaries while those of **3b** and **10** were attached with epoxy cement to a glass fiber. The determination of the Laue symmetry class and an estimation of the unit cell constants were made from an examination of sets of procession photographs obtained with each data crystal. Further examination with an Enraf-Nonius CAD 4 diffractometer indicated that each data crystal had good mosaic

(25) Gilman, H.; Spatz, J. M. *J. Org. Chem.* **1951**, *16*, 1485–1494.
(26) Fieser, L. F.; Williamson, K. L. "Organic Experiments", 3rd ed.; D. C. Health: Lexington, MA, 1975; p 361.
(27) Hart, N. K.; Hoffmann, A.; Lamperton, J. A.; Richards, C. M. *Heterocycles* **1977**, *7*, 265–272.

Scheme I

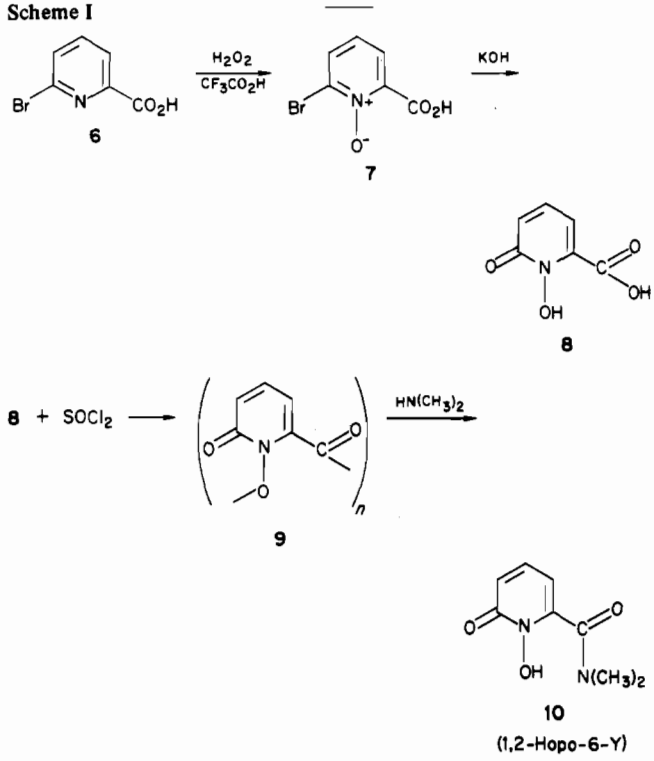

character; the peak widths at half peak height of intense low-angle reflections, as determined by ω scans with an aperture of 1 mm width, were 0.30–0.55, 0.19–0.29, 0.12–0.21, 0.14–0.19, and 0.20–0.29° for crystals of **3a**, **3b**, **4**, **5**, and **10**, respectively. After the accurate centering of 24 high-angle reflections (see Table I) from diverse regions of reciprocal space and the determination of probable space group for each crystal, X-ray intensity data were collected as previously described.[28] Crystal data and data collection parameters that are relevant to these studies are given in Table I. The measured intensities were reduced[28] and assigned standard deviations with the p values given in Table I.

The structures were solved by standard heavy-atom procedures,[29] except for that of **10**, which was solved by direct methods (MULTAN).[28] The structures were refined[28] by full-matrix least-squares methods[30] using only those reflections with $F_o^2 > 3\sigma(F_o^2)$. Neutral-atom scattering factors for all atoms of these structures were used in these calculations and were corrected for anomalous scattering of MoKα radiation.[28]

Potentiometric Titrations. Titrations employed the automatic titrator described previously[20] or were performed manually with a Brinkmann 102 pH meter with Sigma E-4753 or E-4878 ("Trizma") combination electrodes and a calibrated Gilmont 2.0-mL buret for delivery of titrant. Potentiometric titrations were performed in water-jacketed vessels maintained at 25 °C.

Argon was passed through Ascarite to purge it of residual carbon dioxide and was used to degas all solutions before titrations. Carbonate-free KOH solutions (0.1 M standardized with potassium hydrogen phthalate) were prepared from Baker "Dilut-it" ampules and boiled and degassed.

The electrodes were calibrated with acetic acid–potassium acetate buffer (pH ca. 4.5) and dilute nitric acid (pH 2.0–2.5) as described previously;[20] if both calibration solutions have $\mu = 0.100$, then titrations of hydrochloric or acetic acid solutions with the standardized base gave theoretical pH values (within 0.01 pH unit) over the pH range 2–6, and a sodium borate buffer ($\mu = 0.100$) gave the correct pH value of 8.97.[2] Thus electrode linearity over the pH range 2–10 was assumed. As a further check, titrations of acetic acid and **10** were repeated with use of dilute KOH and HNO_3 as electrode calibrants; the pK_a's obtained differed by <0.005 from those using acetate buffer as calibrant.

Spectrophotometric Titrations. All spectra were measured on a Hewlett-Packard 8450A UV–vis multichannel spectrophotometer. A Brinkmann 102 pH meter equipped with a Sigma E-4878 ("Trizma") combination electrode was used. The electrode was calibrated with Mallinckrodt "buffAR" solutions of pH 7.00 and 4.01. Since all equilibrium constants that we report are concentration constants (for ionic strength 0.10), it was necessary to correct the pH readings for differences between the activity scale established by the commercial buffers and the desired concentration pH values. An experimental correction was established by measuring the pH of the commercial buffers with electrodes standardized as in the part on potentiometric titrations (found 6.89 (2) and 3.94 (1)[24]).

During a typical spectrophotometric titration, a solution of iron and ligand originally at pH 5–7 was acidified by addition of small volumes of 1–10 M nitric acid. Spectra were taken every 0.1–0.2 pH unit down to pH 1.5, below which the ionic strength would have been appreciably altered.

EDTA Competition Experiments. Solutions were prepared containing known amounts of iron(III), EDTA, and hydroxypyridinone at pH 4–6 and ionic strength 0.1 M. The spectral changes for the competition with 3,2-Hopo were observed to have a half-time of ca. 20 min. Other solutions were maintained at 25.0 °C for approximately 1 week (2 days for mimosine) to attain equilibrium; the pH and spectra were measured as described in the part on spectrophotometric titrations. Equilibration was ascertained by repeating the measurements a few days later and by agreement in calculated equilibrium constants between solutions in which ferric EDTA had been formed first and solutions in which the EDTA had been added last.

If $Fe(EDTA)^-$ (denoted FeY) and FeL_3 (where L is the deprotonated hydroxypyridinone ligand) are the only iron-containing and only absorbing species, z, the fraction of the iron present as the hydroxypyridinone complex, is given by

$$z = \frac{(\mathrm{Abs}/C_{\mathrm{Fe}}l) - \epsilon_{\mathrm{FeY}}}{\epsilon_{\mathrm{FeL_3}} - \epsilon_{\mathrm{FeY}}}$$

This relation is true at each wavelength, and the HP-8450A is able to calculate z for all wavelengths simultaneously, generating a "spectrum" of z. Theoretically, this should be a horizontal flat line. In fact, the z spectra are relatively flat in the visible absorbance band of FeL_3 with deviations in the UV due to ligand absorbance. The average values of z between 402 and 460 nm were used in calculations, except for the mimosine system, in which the range 460–520 nm was employed.

The concentrations of the various species in solution were calculated from C_{Fe}, z, the total EDTA and hydroxypyridinone concentrations, pH, and known acid dissociation constants. Literature values of acid dissociation constants were used for EDTA and $Fe(EDTA)^{-2}$ and for mimosine (H_2mim) and $Fe(Hmim)_3$.[31] With use of $10^{25.0}$ as the formation constant of FeY,[2] β_3 can be calculated for the reaction

$$Fe^{3+} + 3L^- \underset{\beta_3}{\rightleftharpoons} FeL_3$$

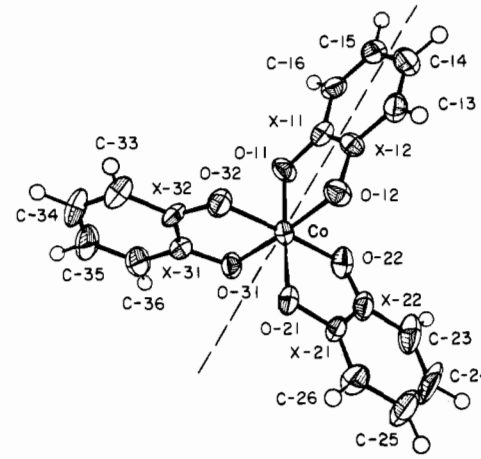

Figure 2. Perspective view of the structure of $Co(1,2\text{-opo})_3$ (**3a**) down a pseudo-C_3 axis of the complex illustrating the atom-numbering scheme. Atoms are drawn as ellipsoids of 50% probability and hydrogen atoms as spheres of radius 0.2 Å. Disordered N/C pairs are indicated by X. The dashed line is a pseudo-C_2 axis in **3a** corresponding to an actual twofold axis in **3b**; atoms in the latter are named as the atoms to the right of this line.

(28) The procedures used for data collection and structure analysis have been described in detail: Eigenbrot, C. W., Jr.; Raymond, K. N. *Inorg. Chem.* **1982**, *21*, 2653–2660.
(29) The positions of an oxygen atom as well as that of Fe(III) were obtained from the Patterson maps for **4** and **5**.
(30) The function minimized in refinement is $\sum w(|F_o| - |F_c|)^2$, where the weight w is $4F_o^2/\sigma^2(F_o^2)$.
(31) Tsai, W.-C.; Ling, K.-H. *J. Chin. Biochem. Soc.* **1973**, *2*, 70–86.

Table II. Final Positional Parameters and B_{eq} Values for Non-Hydrogen Atoms for Both Structures of Co(1,2-opo)$_3$ (3a and 3b)[24] [b]

atom [N occ] [a]	x	y	z	B_{eq}, Å^2
		Structure 3a ($P2_1/n$)		
Co	−0.14009 (6)	0.22893 (6)	0.11194 (4)	2.170 (9)
O11	−0.1304 (3)	0.0827 (3)	0.0399 (2)	2.88 (7)
O12	−0.1705 (3)	0.0882 (3)	0.1831 (2)	2.83 (7)
O21	−0.1432 (3)	0.3692 (3)	0.1888 (2)	2.75 (7)
O22	0.0567 (3)	0.2202 (4)	0.1553 (2)	3.32 (7)
O31	−0.1167 (3)	0.3643 (3)	0.0356 (2)	2.71 (7)
O32	−0.3364 (3)	0.2459 (3)	0.0676 (2)	2.88 (7)
X11 [0.66 (2)]	−0.1333 (4)	−0.0403 (4)	0.0767 (2)	2.47 (8)
X12 [0.34 (3)]	−0.1529 (4)	−0.0373 (4)	0.1528 (3)	2.27 (8)
C13	−0.1556 (5)	−0.1606 (5)	0.1936 (3)	3.0 (1)
C14	−0.1371 (5)	−0.2830 (6)	0.1595 (3)	3.6 (1)
C15	−0.1178 (5)	−0.2883 (5)	0.0809 (3)	3.3 (1)
C16	−0.1157 (5)	−0.1661 (5)	0.0405 (3)	2.8 (1)
X21 [0.46 (3)]	−0.0157 (4)	0.3744 (4)	0.2395 (2)	2.66 (8)
X22 [0.54 (3)]	0.0881 (4)	0.2941 (5)	0.2210 (3)	3.09 (9)
C23	0.2216 (5)	0.2976 (7)	0.2723 (3)	4.7 (1)
C24	0.2461 (6)	0.3797 (8)	0.3395 (4)	6.1 (2)
C25	0.1393 (6)	0.4586 (7)	0.3578 (4)	5.4 (2)
C26	0.0066 (6)	0.4571 (6)	0.3068 (3)	3.7 (1)
X31 [0.48 (3)]	−0.2417 (4)	0.3882 (4)	−0.0142 (2)	2.53 (8)
X32 [0.52 (3)]	−0.3562 (4)	0.3244 (5)	0.0018 (2)	2.75 (9)
C33	−0.4884 (6)	0.3419 (7)	−0.0491 (4)	4.4 (1)
C34	−0.5004 (6)	0.4253 (7)	−0.1149 (4)	5.5 (2)
C35	−0.3852 (6)	0.4935 (7)	−0.1294 (3)	4.8 (1)
C36	−0.2549 (6)	0.4746 (6)	−0.0800 (3)	3.9 (1)
		Structure 3b ($C2/c$)		
Co	0.000	0.22811 (5)	0.250	3.14 (1)
O12	0.0241 (1)	0.0836 (2)	0.3673 (1)	4.06 (4)
O21	0.02726 (9)	0.3646 (2)	0.3742 (1)	3.23 (3)
O22	0.1215 (1)	0.2362 (2)	0.2251 (2)	4.09 (4)
X12 [0.500 00]	0.0135 (1)	−0.0409 (2)	0.3118 (2)	3.44 (5)
C13	0.0277 (2)	−0.1652 (3)	0.3746 (2)	4.12 (6)
C14	0.0136 (2)	−0.2886 (2)	0.3131 (3)	4.64 (6)
X21 [0.55 (2)]	0.1145 (1)	0.3830 (2)	0.3911 (2)	3.36 (5)
X22 [0.45 (1)]	0.1640 (2)	0.3141 (3)	0.3123 (2)	3.99 (5)
C23	0.2551 (2)	0.3311 (4)	0.3269 (3)	6.22 (8)
C24	0.2931 (2)	0.4154 (5)	0.4181 (3)	8.1 (1)
C25	0.2424 (2)	0.4846 (4)	0.4969 (3)	7.20 (9)
C26	0.1535 (2)	0.4677 (3)	0.4832 (3)	4.85 (7)

[a] Number in brackets is refined fractional N occupancy. The remainder of the occupancy is made up of a C atom with identical positional and thermal parameters. [b] See Figure 2 for identity of the atoms.

Table III. Final Positional Parameters and B_{eq} Values for Fe(1,2-opo)$_3$ (4)[24] [a]

atom	x	y	z	B_{eq}, Å^2
Fe	0.0000 (0)	0.0000 (0)	0.2500 (0)	1.743 (6)
O1	0.0616 (1)	0.1921 (1)	0.28721 (3)	2.52 (2)
N1/C1	0.0320 (1)	0.2998 (2)	0.27005 (7)	2.15 (4)
C2	0.0631 (2)	0.4389 (2)	0.29057 (5)	3.16 (3)
C3	0.0319 (2)	0.5454 (2)	0.27069 (6)	3.85 (4)
H2	0.104 (2)	0.453 (2)	0.3176 (6)	4.6 (5)
H3	0.046 (2)	0.633 (2)	0.2862 (7)	5.5 (5)

[a] N1 and C1 are present at half-occupancy and are constrained to have the same positional and thermal parameters. See Figure 3 for identity of the atoms.

Several samples of varying total metal and ligand concentrations were prepared and the values of β_3 averaged.

Results

Structure Determinations. The atom-numbering schemes are shown in ORTEP views of the final structures presented in Figures 2–5.[28] Tables II–V provide the atomic positional parameters with esd's, as derived from the least-squares inverse matrix, for the structures of **3a/b**, **4**, **5**, and **10**, respectively. Selected bond lengths are given in Tables VI–IX. Tables of anisotropic thermal parameters (Tables X–XIII), hydrogen atom parameters for **3a/b** and **10** (Tables XIV and XV), and observed and calculated structure factor amplitudes (Tables XVI–XIX) are available.[32]

(32) See statement at end of paper regarding supplementary material.

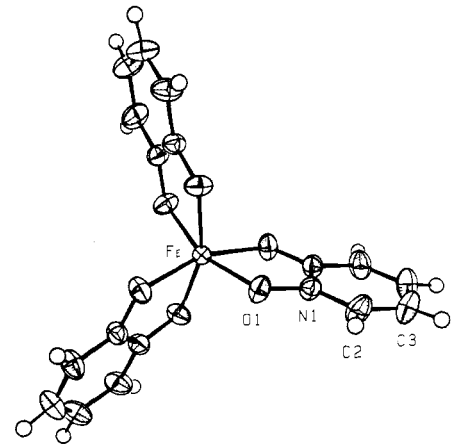

Figure 3. Perspective view of the structure of Fe(1,2-opo)$_3$ (**4**) down the C_3 axis of the complex illustrating the atom-numbering scheme. Atoms are drawn as ellipsoids of 50% probability and hydrogen atoms as spheres of radius 0.2 Å.

Co(1,2-opo)$_3$ (3a and 3b). Growth of untwinned single crystals of the cobalt complex proved very difficult. Two crystals were examined on the diffractometer. The first of these (**3a**) was assigned space group $P2_1/n$ based on precession photographs and a data set collected on the diffractometer. Azimuthal scans of three of five reflections examined showed large (~40%) variations in intensity that could not be explained by crystal absorption (5%

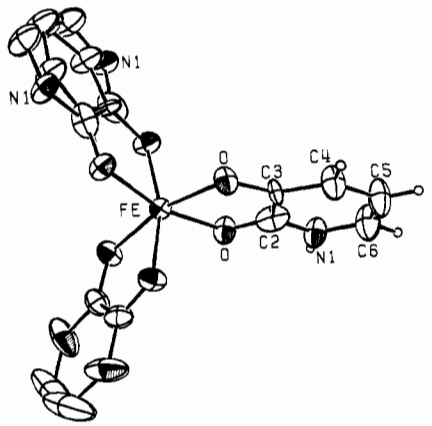

Figure 4. Perspective view of the structure of $Fe(3,2\text{-opo})_3$ (**5**) down the C_3 axis of the complex. The ligand at the right is a single half-occupancy ring with the atom-numbering scheme shown. At the upper left the relative positions of the two half-occupancy rings are illustrated. The ligand at lower left illustrates the large thermal parameters that resulted from the five-atom refinement (similar to the $Fe(1,2\text{-opo})_3$ structure). Atoms are drawn as ellipsoids of 50% probability and hydrogen atoms as spheres of radius 0.1 Å.

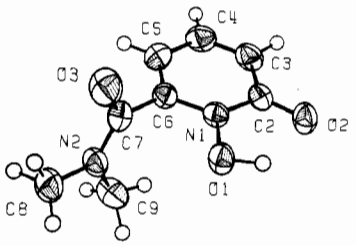

Figure 5. Perspective view of the structure of 1,2-Hopo-6-Y (**10**) illustrating the atom-numbering scheme. Atoms are drawn as ellipsoids of 50% probability and hydrogen atoms as spheres of radius 0.2 Å.

Table IV. Positional Parameters and B_{eq} Values for $Fe(3,2\text{-opo})_3$ (**5**)[24a]

atom	x	y	z	B, Å²
Fe	0.000	0.000	0.250	1.977 (5)
O	−0.0696 (1)	−0.1917 (1)	0.21061 (3)	2.69 (2)
N1	−0.0882 (3)	−0.4280 (3)	0.20372 (8)	2.88 (5)
C2	−0.0423 (4)	−0.2958 (4)	0.22480 (9)	3.13 (7)
C3	0.0321 (3)	−0.2610 (2)	0.26847 (8)	1.86 (4)
C4	0.0512 (3)	−0.3849 (3)	0.2864 (1)	3.39 (6)
C5	0.0044 (4)	−0.5240 (3)	0.2622 (1)	4.13 (8)
C6	−0.0645 (4)	−0.5421 (4)	0.2211 (1)	3.98 (7)
H1[b]	−0.1343	−0.4431	0.1783	5.0
H4[b]	0.0960	−0.3734	0.3156	5.0
H5[b]	0.0209	−0.6046	0.2742	5.0
H6[b]	−0.0969	−0.6364	0.2044	5.0

[a] In this refinement all atoms except Fe and O are at half-occupancy. See Figure 4 for identity of the atoms. A hydrogen atom is named in accordance with the carbon or nitrogen atom to which it is bonded. [b] Atoms included but not refined.

variation calculated based on crystal shape); this and the relatively large peak widths observed in ω scans probably indicates the crystal had fractured.

In order to get a more accurate structure, additional crystals were grown from a variety of solvent systems. Crystals from CH_2Cl_2–MeOH gave crystals with well-defined faces, although many exhibited obvious twinning. A visually satisfactory crystal with a well-defined Laue photograph (**3b**) was examined on the diffractometer, where an automated search procedure found a *C*-centered monoclinic unit cell as indicated in Table I. However, subsequent examination revealed several weak low θ reflections with half-integral indices or $h + k = 2n + 1$.

The volume and b length for crystals **3a** and **3b** are nearly identical, and other lengths and angles indicate $a_{3b} = {}^3/_2 a_{3a} + {}^1/_2 c_{3a}$ and $c_{3b} = -{}^1/_2 a_{3a} + {}^1/_2 c_{3a}$. The intensities of the weak anomalous reflections in crystal **3b** are proportional to corresponding strong reflections for crystal **3a**, consistent with the hypothesis that crystal **3b** contains a 1% twin of the $P2_1/n$

Table V. Final Positional Parameters and B_{eq} Values for Non-Hydrogen Atoms of 1,2-Hopo-6-Y (**10**)[24a]

atom	x	y	z	B_{eq}, Å²
O1	0.408 18 (6)	0.1138 (2)	0.8317 (3)	3.93 (3)
O2	0.544 36 (7)	0.0643 (2)	0.7811 (3)	4.05 (3)
O3	0.324 49 (9)	0.4302 (2)	0.7309 (4)	5.50 (4)
N1	0.444 22 (7)	0.1933 (2)	0.6552 (3)	2.97 (3)
N2	0.277 49 (8)	0.2433 (2)	0.4781 (3)	3.59 (3)
C2	0.405 08 (10)	0.2938 (2)	0.5067 (4)	3.08 (4)
C3	0.436 40 (12)	0.3702 (2)	0.3186 (4)	3.98 (4)
C4	0.507 91 (11)	0.3420 (2)	0.2844 (4)	4.26 (4)
C5	0.545 90 (10)	0.2422 (2)	0.4370 (4)	3.89 (4)
C6	0.515 12 (9)	0.1600 (2)	0.6340 (4)	3.15 (4)
C7	0.331 10 (10)	0.3258 (2)	0.5829 (4)	3.43 (4)
C8	0.205 28 (11)	0.2714 (3)	0.5468 (5)	5.15 (5)
C9	0.285 98 (12)	0.1177 (3)	0.3106 (5)	4.81 (5)

[a] See Figure 5 for identity of the atoms.

Table VI. Selected Interatomic Distances (Å) and Angles (deg) for $Co(1,2\text{-opo})_3$ Structures 3a and 3b[24c]

3b ($C2/c$)		3a ($P2_1/c$)			
		Distances			
Co-O12	1.882 (1)	Co-O12	1.880 (2)	Co-O11	1.878 (2)
Co-O21	1.885 (1)	Co-O21	1.881 (2)	Co-O31	1.887 (2)
Co-O22	1.889 (1)	Co-O22	1.883 (2)	Co-O32	1.887 (2)
O12-X12	1.330 (2)	O12-X12	1.329 (3)	O11-X11	1.334 (4)
X12-X12′	1.359 (3)			X11-X12	1.362 (4)
O12-O12′	2.572 (3)			O11-O12	2.575 (3)
O21-X21	1.327 (2)	O21-X21	1.338 (3)	O31-X31	1.331 (3)
O22-X22	1.315 (2)	O22-X22	1.302 (4)	O32-X32	1.330 (4)
X21-X22	1.361 (2)	X21-X22	1.359 (4)	X31-X32	1.349 (4)
O21-O22	2.573 (2)	O21-O22	2.573 (3)	O31-O32	2.580 (3)
		O-Co-O Angles			
O12, O12′	86.20 (8)			O11, O12	86.48 (9)
O21, O22	85.99 (6)	O21, O22	86.2 (1)	O31, O32	86.25 (9)
O12, O21′	176.54 (6)	O12, O31	176.6 (1)	O11, O21	176.7 (1)
O22, O22′	175.32 (9)			O22, O32	177.6 (1)
		Trigonal Twist Angle (ϕ)[a]			
55.7		56.4 (calcd 54.9)[b]			

[a] The trigonal twist angle is obtained by averaging the three torsion angles defined by the centroids CEN(1) and CEN(2) of the faces "normal" to the molecular pseudo-C_3 axis and the pairs of oxygen atoms composing each chelate ring, e.g., O(n1)/CEN(1)/CEN(2)/O(n2). [b] The average of three values given by the expression $\phi = -73.9 + 94.10b$, where b is the ratio of O···O distance within a chelate ring to the metal-O bond length (see ref 54 and references therein). [c] See Figure 2 for identity of atoms.

Table VII. Selected Interatomic Distances (Å) and Angles (deg) for $Fe(1,2\text{-opo})_3$ (**4**)[a]

Fe-O1	2.008 (1)	C2-C3	1.356 (2)
O1-N1	1.320 (2)	C3-C3′	1.400 (3)
N1-C1	1.364 (3)	O1···O1′	2.545
N1-C2	1.377 (2)		
cis O1-Fe-O1	78.63 (5)	N1-C2-C3	120.00 (14)
	89.77 (3)	C2-C3-C3′	119.81 (8)
	105.06 (5)	obsd trigonal twist angle (ϕ)[b]	36.6
trans O1-Fe-O1	160.97 (5)		
C1-N1-C2	120.18 (9)	calcd trigonal twist angle[b]	45.4

[a] Numbers in parentheses are the estimated standard deviations in the least significant digits. See Figure 3 for identity of the atoms. Positions of atoms O1, N1, C2, and C3 are related, in the same order, to the positions of atoms O1′, C1, C2′, and C3′ by the C_2 axis that passes through the Fe position and the midpoints of the N1–C1 and C3–C3′ bonds (see text). [b] Defined in footnotes *b* and *c* of Table VI.

Table VIII. Selected Interatomic Distances (Å) and Angles (deg) for Fe(3,2-opo)$_3$ (5)[a]

Fe-O	2.016 (1)	C5-C6	1.358 (7)
O-C2	1.248 (9)	N1-C6	1.350 (5)
O-C3	1.366 (8)	O-O	2.615 (2)
N1-C2	1.297 (10)	O-N1[b]	2.850 (3)
C2-C3	1.439 (4)	C2-C3'[c]	0.22 (2)
C3-C4	1.418 (9)	N1-C4'[c]	0.502 (4)
C4-C5	1.397 (5)	C5-C6'[c]	0.728 (5)
cis O-Fe-O	80.85 (5)	N1-C2-C3	123.4 (9)
	89.87 (4)	C2-C3-C4	113.6 (8)
	101.30 (5)	obsd trigonal twist angle (ϕ)[d]	42.1
trans O-Fe-O	165.39 (5)		
C2-N1-C6	121.6 (6)	calcd trigonal twist angle[d]	47.5
C3-C4-C5	121.4 (6)		
C4-C5-C6	119.1 (4)		
C5-C6-N1	120.9 (4)		

[a] Numbers in parentheses are the computed esd's in the least significant digits. Because of high correlation between C2 and C3, bond lengths involving these atoms are certainly much less accurate than suggested by computed esd's. [b] Intermolecular hydrogen bond. [c] Primed atoms are on half-occupancy ligands different from those of their unprimed counterparts to which they are related by the twofold rotation axes passing through the iron. [d] Defined in footnotes *b* and *c* of Table VI.

Table IX. Selected Interatomic Distances (Å) for 1,2-Hopo-6-Y (10)[a]

O1-N1	1.378 (1)	C6-C7	1.509 (2)
O2-C2	1.241 (2)	C7-O3	1.230 (2)
N1-C2	1.383 (1)	C7-N2	1.327 (2)
C2-C3	1.412 (2)	N2-C8	1.458 (2)
C3-C4	1.351 (2)	N2-C9	1.450 (2)
C4-C5	1.398 (2)	O1-HO1	1.00[b]
C5-C6	1.356 (2)	O1···O2	2.640 (1)
N1-C6	1.356 (2)	O2···HO1	1.98[b]

[a] Numbers in parentheses are the estimated standard deviations in the least significant digits. See Figure 5 for identity of the atoms. [b] The position of atom HO1 was not refined but estimated from a difference Fourier map.

structure. For this reason crystal **3b** was treated as *C*-centered monoclinic (the unattractive alternative would have been to postulate a primitive monoclinic cell with $Z = 8$).

Refinement of an isotropic model for structure **3a** in which all six atomic positions of each pyridinone ring were treated as carbon atoms failed to distinguish clearly between the oxygen-bonded carbon and nitrogen positions.[33] This suggested that the crystal is disordered, perhaps with a mixture of cis and trans isomers. This is probed more closely below. Least-squares refinement of a model (anisotropic) in which hydrogen atoms were held at idealized positions[34,35] gave $R = 0.063$, $R_w = 0.071$, and $E = 2.09$[36] for 2589 observations and 229 variables. In the concluding cycles of refinement the fractional nitrogen (vs. carbon) occupancy of the atoms bonded to the oxygens in the three pyridinone rings were refined (constrained so that the sum of N occupancy is 1.0 for each ligand). In the final cycle of refinement, the largest parameter shift was 0.19 times the estimated standard deviation (esd) of an occupancy parameter of one of the disordered N/C positions; all positional shifts were less than 0.09 of a corresponding esd. The six largest peaks on a final difference Fourier map were 0.7–1.7 e Å^{-3} and were 0.2–1.0 Å from the Co(III) position.[37] For comparison, the oxygen atoms exhibited heights of 9.8–11.8 e Å^{-3} on the heavy-atom map. Examination of $|F_o|$ vs. $|F_c|$ as a function of magnitude of $|F_o|$, setting angles, and Miller index showed the greatest disagreement for intense, low-angle $h0l$ reflections ($|F_o| > |F_c|$). Comparison of $|F_o|$ and $|F_c|$ for the low-angle reflections gave no evidence of secondary extinction.

The C_2 axis of **3b** passes through the metal and one of the ligands of the Co(1,2-opo)$_3$ molecule (Figure 2). This imposes disorder of the nitrogen and a carbon in one of the ligands; the other two symmetry-related ligands were found to be similarly disordered and occupancies refined in a fashion similar to those of **3a**. Hydrogen atoms (located in a difference electron density map) were included at idealized positions; all other atoms were refined anisotropically to give $R = 0.024$, $R_w = 0.031$, and $E = 1.64$ for 882 observations and 115 variables. The largest peak in the final difference Fourier synthesis was <0.2 e Å^{-3}. Examination of $|F_o|$ vs. $|F_c|$ as a function of $|F_o|$, θ, and Miller index showed no anomalies.

Fe(1,2-opo)$_3$ (4). Acentric space group $R3c$ can accommodate six Fe(III) ions per unit cell at sites of $C_3(3)$ symmetry, while centric space group $R\bar{3}c$ requires that the six metal ions occupy sites of either $S_6(\bar{3})$ or $D_3(32)$ symmetry. Since the last two choices are inconsistent with the symmetry of the complex, the structure was solved and initially refined in the acentric space group. Although refinement of a model structure in which all atoms of the pyridinone ring were designated as carbon and in which the thermal motions of all non-hydrogen atoms were treated anisotropically yielded low error indices (0.045 and 0.071 for R and R_w, respectively) and satisfactory molecular geometry, it would not converge. Moreover, inspection of the atomic coordinates clearly revealed that the positions of the two oxygen atoms and of pairs of carbon atoms of the pyridinone ring were very nearly related by the C_2 axis that bisects the ring and passes through the Fe(III) position. Thus, the coordinates of the atoms were transformed to those that correspond to D_3 symmetry in space group $R\bar{3}c$ (hexagonal setting). Convergence of an anisotropic model was quickly attained with R and R_w indices of 0.038 and 0.060, respectively. Inclusion in refinement of the ring hydrogen atoms at positions determined from a difference electron density map lowered the error indices to 0.036 and 0.058. Assignment of half-occupancy nitrogen and half-occupancy carbon atoms to the positions of the atoms of the pyridinone ring that are bonded to the oxygen atoms, followed by additional refinement, which included a correction for secondary extinction[38] (6.88 (11) × 10^{-7} e^{-2}), led to convergence with $R = 0.021$, $R_w = 0.035$, and $E = 1.65$ for 556 observations and 48 variables. In the last cycle of refinement the largest shift in a parameter was 0.15 of a corresponding esd. The largest peak on a final difference electron density map was 0.24 e Å^{-3}. Examination at the end of refinement of $|F_o|$ vs. $|F_c|$ as a function of the magnitude of $|F_o|$, $(\sin\theta)/\lambda$, and Miller index showed no anomalies.

Fe(3,2-opo)$_3$ (5). Solution and refinement of this structure presented the same kind of dilemma as was encountered for **4**, namely, that although an ordered structure could be described in the acentric space group $R3c$, the resulting molecular geometry was unacceptable (N1–C6 = 1.72 Å, C4–C5 = 1.20 Å; see Figure 4 for the numbering scheme) and at least four possible least-squares minima with low R values ($R = 0.041$–0.044; $R_w = 0.054$–0.059; hydrogen atoms not included) were found, corre-

(33) The refined isotropic thermal parameters for these adjacent positions of the three pyridinone rings, when all atoms were assigned carbon scattering factors, were 1.7 and 2.2 Å^2, 2.1 and 2.3 Å^2, and 2.0 and 2.3 Å^2, respectively.
(34) The C–H distances were constrained to 0.95 Å in accordance with a previous study[35] and assigned fixed thermal parameters of 5.0 Å^2.
(35) Churchill, M. R. *Inorg. Chem.* **1973**, *12*, 1213–1214.
(36) The error indices R, R_w, and the error in an observation of unit weight E are defined in ref 28.
(37) Crystal fracturing probably causes the large R values and difference Fourier peaks. The alternate hypothesis of twinning by **3b** (unnoticed at the time of crystal examination) was explored. Such twinning would be expected to cause $|F_o| > |F_c|$ for $3h + 2k + l = 4n$ reflections, which was generally observed. Refinement of 1917 reflections with $F_o^2 > 3\sigma(F_o^2)$ and $3h + 2k + l \neq 4n$ gave $R = 0.052$, $R_w = 0.061$, $E = 1.716$, and largest peaks in the difference electron density map of 0.6 e/Å^3. Bond lengths and nitrogen occupancies were not substantially different from those of the structure reported. It should be noted that the three reflections showing large intensity variations in the azimuthal scans were $3h + 2k + l \neq 4n$, so that the twinning hypothesis cannot account for these disturbing observations.
(38) Zachariasen, W. H. *Acta Crystallogr., Sect. A: Cryst. Phys., Diffr., Theor. Gen. Crystallogr.* **1968**, *A24*, 212–216.

Table XX. Acid Dissociation Constants of Hydroxypyridinones[24]

ligand	$pK_{a,1}$	$pK_{a,2}$	ionic strength	temp, °C	ref
1,2-Hopo	5.78 (2)		0.1	25	this work
	5.81	−0.9	0.1	25	41
1,2-Hopo-6-Y	5.17 (1)		0.1	25	this work
3,2-Hopo	8.66 (1)		0.1	25	this work
	8.69	0.11	1.0	25	42
	8.66	0.2	0.15	37	43
3,4-Hopo	9.01 (1)	3.34 (1)	0.1	25	this work
	9.01	3.36	0.15	37	43

sponding to enantiomers and exchange of identities of N1 and C4. However, the five-atom $R\bar{3}c$ (hexagonal setting) model similar to the Fe(1,2-opo)$_3$ model converged with significantly higher R = 0.054, R_w = 0.075. No hydrogen atoms could be located on difference Fourier maps because of large (0.5–0.9 e/Å^3) peaks associated with the disordered N1/C4 and C5/C6 pairs.

A significantly better structure was obtained with an eight-non-hydrogen atom $R\bar{3}c$ model in which disorder was assumed but in which C3, C4, and C5 were not constrained to be symmetry related to C2, N1, and C6, respectively. This model invokes two half-occupancy rings that are related by the twofold axis (see Figure 4).[39]

Refinement using this structure gives R = 0.032, R_w = 0.050; inclusion of hydrogen atoms (located—except H6—in the difference Fourier map; placed at idealized positions[34]) and refinement of the secondary extinction parameter (4 (1) × 10^{-7} e^{-2})[38] gives a final R = 0.024, R_w = 0.035, and E = 1.44 for 629 observations and 67 variables. Correlations between positional parameters of C2 and C3 averaged 0.91 while those between N1 and C4 were ca. 0.7. The largest peak in the final difference Fourier map was at the origin (0.30 e Å^{-3}). No discrepancies as a function of $|F_o|$, (sin θ)/λ, or Miller index were noted upon comparison of $|F_o|$ with $|F_c|$.

1,2-Hopo-6-Y (10). Full-matrix least-squares refinement of the structure, in which all non-hydrogen atoms were refined anisotropically while hydrogen atoms, all of which were located from a difference Fourier map, were held at idealized positions,[34,40] converged with R = 0.041, R_w = 0.061, and E = 2.60 for 1183 observations and 119 variables. A correction (1.7 (4) × 10^{-6} e^{-2}) for secondary extinction[38] was applied in the concluding cycles of refinement. In the final cycle of refinement all shifts in parameters were less than 0.01 of a corresponding esd. The largest peaks on a final difference electron density map were ~0.2 e Å^{-3}. There were no trends in $|F_o|$ and $|F_c|$ as a function of $|F_o|$, (sin θ)/λ, or Miller index.

Solution Equilibria. Potentiometric Titrations. Table XX shows the acid dissociation constants determined from potentiometric titrations of solutions of the various ligands at 25 °C and μ = 0.1. Also shown are values from the literature for different conditions.[41–43] For 3,4-Hopo both the protonation and the deprotonation of the neutral ligand were observed; for the other ligands no effort was made to determine the constant for the protonation of the neutral ligand (a value of 0.1 was used for the low pK_a of 3,2-Hopo in all calculations). The nonlinear least-squares program BETA[44] was used for the refinement of the potentiometric data.

When a solution containing a 3:1 ratio of 1,2-Hopo-6-Y to iron(III) (0.7 mM) is titrated with base, a strong acid titration

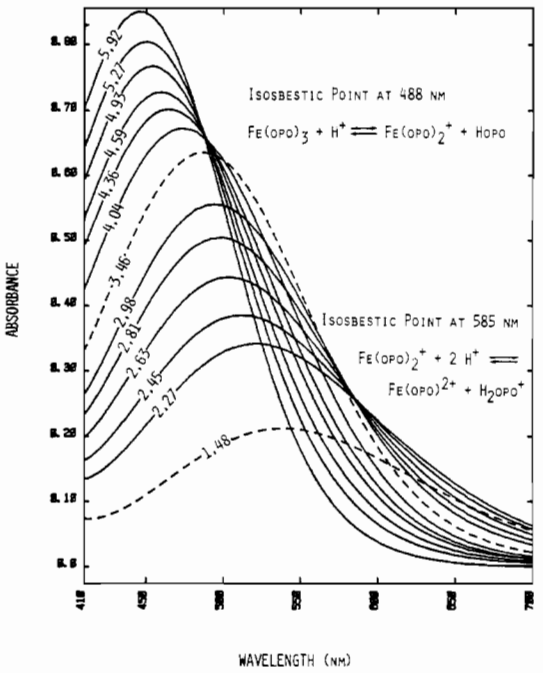

Figure 6. Spectra observed in the course of a typical spectrophotometric titration of hydroxypyridinone/iron systems with a ligand to metal ratio of at least 3. In this case, the ligand is 3,4-Hopo, which was chosen for the illustration because the spectral crossing angle at the 585-nm isosbestic point is the largest and hence is the easiest to see. The solution is 0.020 mF iron(III) and 0.080 mF ligand, and the spectra are taken through a 10.0-cm cell.

curve with inflection point at 3 equiv of base/equiv of iron indicates the liberation of three protons upon complexation, consistent with FeL_3 formation. As the fourth through sixth equivalents of base were added, equilibration became slow, the pH buffered between 7 and 9, and precipitate appeared, presumably $Fe(OH)_3$. The initial pH of the titration solution (2.6) indicates 2.75 protons were released upon mixing of the ligand with the iron stock solution. Assuming that FeL_3 and FeL_2^+ are the predominant iron species in solution at low pH, it is possible to refine log K_3 = 6.9 (1).[24]

Because of the high degree of complexation observed in the 3:1 ligand to metal system, no effort was made to measure K_2 or K_1 by potentiometric methods. Furthermore, the low solubilities of the iron complexes of the unsubstituted hydroxypyridinones precluded any potentiometric analysis of the solution chemistry of these species.

Spectrophotometric Titrations. The extinction coefficients and wavelength maxima for the FeL^{2+}, FeL_2^+, and FeL_3 complexes of hydroxypyridinone ligands, as well as of catechol,[45] are shown in Table XXI. In all cases the FeL_3 complex has a molar absorptivity of ca. 4000 M^{-1} cm^{-1}, which decreases as the ligands dissociate and the position of the absorption band moves to lower energy. These changes in the visible spectrum allowed the determination of stepwise formation constants spectrophotometrically.

As mentioned above, the neutral tris(hydroxypyridinonato) iron is quite insoluble for all three unsubstituted isomers. Solutions more than 2 × 10^{-5} M in FeL_3 were liable to precipitate; once precipitation began, the concentration of iron in solution dropped over several hours to an equilibrium level below 10 μM. To compensate for the low concentrations, longer optical cells (10.0-cm path lengths) were used for spectrophotometric titrations. The high dilutions were also important to bring the dissociation equilibria into the pH range observable at ionic strength 0.1.

As a result of the low concentrations employed, it became very important to use glassware and supporting electrolyte medium free of metal contaminants. Solutions of 3,2-Hopo with iron

(39) An attempt was made to refine two half-occupancy oxygen atoms. Positional correlations between the two oxygen atoms were 0.99, and unreasonable Fe–O bond lengths (1.89 and 2.13 Å) resulted. Thus a single full-occupancy oxygen was included in the final structure.

(40) The hydrogen atom of the hydroxyl group bonded to the nitrogen atom of the pyridinone ring was maintained at its position estimated from a difference map.

(41) Sun, P. J.; Fernando, Q.; Freiser, H. *Anal. Chem.* **1964**, *36*, 2485–2488.
(42) Curtis, K. E.; Atkinson, G. F. *Can. J. Chem.* **1972**, *50*, 1649–1654.
(43) Stünzi, H.; Perrin, D. D.; Teitei, T.; Harris, R. L. N. *Aust. J. Chem.* **1979**, *32*, 21–30; **1980**, *33*, 2207–2220.
(44) Harris, W. R.; Carrano, C. J.; Cooper, S. R.; Sofen, S. R.; Avdeef, A.; McArdle, J. V.; Raymond, K. N. *J. Am. Chem. Soc.* **1979**, *101*, 6097–6104.
(45) Avdeef, A.; Sofen, S. R.; Bregante, T. L.; Raymond, K. N. *J. Am. Chem. Soc.* **1978**, *100*, 5362–5370.

Table XXI. Visible and Near-Ultraviolet Absorption Maxima (nm) and Extinction Coefficients (cm^{-1} M^{-1}, in Parentheses) of FeL^{2+}, FeL_2^+, and FeL_3, Where L Represents Hydroxypyridinone Ligands and Positions of the Isosbestic Points[a]

ligand	FeL^{2+}		FeL_2^+		FeL_3	FeL_3 (KBr)
1,2-Hopo	470 (1750)		447 (3120)		412 (4310)	416
isos pts		530 (1070)		460 (3040)		
1,2-Hopo-6-Y	470 (1920)		450 (3220)		417 (4490)	422
isos pts		528 (1180)		464 (3100)		
3,2-Hopo	600 (1810)		548 (3690)		502 (5160)	514
			415 (1880)		417 (4080)	414
isos pts		669 (1440)		556 (3670)		
3,4-Hopo	538 (1550)		488 (3310)		446 (4320)	
isos pts		582 (1360)		488 (3310)		
catechol	700 (1500)		570 (3330)		490 (4190)	
			385 (1900)			

[a] For comparison, the values for FeL^+, FeL_2^-, and FeL_3^{3-} (L = catechol) are shown. The last column shows absorbance maxima for a KBr pellet of powdered FeL_3; all other values are for aqueous solution, $\mu = 0.1$, $T = 25$ °C.

Table XXII. Conditions for the Spectrophotometric Titrations and Results of Data Refinements[e]

ligand	1,2-Hopo		1,2-Hopo-6-Y		3,2-Hopo				3,4-Hopo		
C_{Fe}, mM	0.0212	0.0348	0.0216	0.250	0.0249	0.0200	0.0233	0.0400	0.0196	0.0200	0.0248
C_L, mM	0.0899	0.1196	0.0862	0.869	0.2485	4.32	17.11	0–0.06[d]	0.0697	0.0801	0.0993
special conditions				1-cm cell		0.1 M $NaClO_4$	0.1 M $NaClO_4$	0.1 M $NaClO_4$		23 °C	
approx pH of pptn[a]	7.1		6.3		7.6					>9.2	
no. of spectra refined	18	9	25	15	25	49	29	15	24	20	17
pH range refined values	4.9–1.7	6.4–3.2	5.1–1.4	4.1–2.5	6.8–1.6	2.4–11.0	11.4–5.9	2.27	5.5–1.9	5.6–1.6	1.0–3.0
log K_1	nr[b]	nr	nr	nr	11.48 (4)	nr	nr	11.76 (4)	nr	14.26 (3)	14.21 (1)
log K_2	9.04 (1)	nr	8.54 (15)	nr	9.77 (1)	nr	nr	nr	11.57 (1)	11.47 (1)	11.65 (1)
log K_3	7.55 (1)	7.63 (6)	7.11 (2)	7.08 (2)	8.01 (1)	8.15 (1)	nr	nr	9.39 (1)	9.18 (1)	nr
pK_a's of ML_3	...	...	...	...	...	9.03 (2)	9.06 (1)	...	...	...	...
	...	...	...	...	...	10.8 (1)	11.23 (2)	...			
av error in[c] abs measmt	0.0005	0.0032	0.0016	0.0007	0.0019	0.0021	0.0017	0.0010	0.0009	0.0021	0.0014
no. of parameters/ no. of variables	5.1	4.0	6.7	6.7	6.7	10.3	8.7	5.0	6.9	5.3	6.8

[a] Kinetically slow decrease in absorbance observed in attempted titrations under similar conditions. [b] nr = not refined. [c] Average error is defined as $\{[\Sigma(Abs_{calcd} - Abs_{obsd})^2]/(N_{observns} - N_{var})\}^{1/2}$, where $N_{observns}$ is the number of observations (four absorbance values at each pH) and N_{var} is the number of refined variables. This function is minimized by the least-squares program. [d] Ligand solution added at constant pH. [e] The esd's of the last digit are in parentheses. Titrations were performed at 25.0 °C and in 0.1 M KNO_3 with use of 10.0 cm optical path length, except as indicated.

changed in visible absorption on standing in air for several hours, presumably due to air oxidation (3,2-Hopo air oxidizes in iron-free basic solution to give a reddish solution with λ_{max} 384 and 402 nm); hence titrations were conducted under an argon atmosphere in an all-glass apparatus.

Figure 6 shows the changes in the visible spectrum as concentrated acid is added to 2.0×10^{-5} M ferric ion with 4 equiv of 3,4-Hopo. There are two temporary isosbestic points observed during the titration; the first occurs between pH 6 and 4 at 488 nm and the second between pH 3 and 2 at 585 nm. Below pH 2, the absorbance decreases throughout the spectrum. This behavior is indicative of three stepwise dissociations from the initially present complex to give the virtually colorless hexaaquoiron species. Similar behavior is observed with solutions of iron and the other hydroxypyridinones, although the low-pH isosbestic point is less well-defined due to a very acute crossing angle.

Estimates of the equilibrium constants were made on the basis of the pH ranges at which the various isosbestic processes occurred. These estimates were refined by a nonlinear least-squares program which refined on absorbance values and treated pH and volume of dilution (usually less than 1% of the total volume) as the independent variables. The absorbance spectra were averaged over wavelength ranges of approximately 50 nm (this is the average from 25 signal detectors on the HP-8450A multichannel spectrophotometer); absorbances and extinction coefficients (as refined parameters) from four wavelength ranges were used in the refinements. With the long path length cells, apparently random changes in absorbance of up to 0.001 absorbance unit were noted between successive spectra even with only water in the cells; the effects of this baseline drift could be largely corrected by subtracting from each spectrum its average absorbance in a low-absorbing region (750–800 nm for the titrations with 3,2-Hopo and 700–800 nm for the others).

The results of the spectrophotometric titrations and subsequent data refinements are summarized in Table XXII. It was not possible to refine K_1 of 1,2-Hopo and 1,2-Hopo-6-Y since the 1:1 complex of these ligands with iron does not dissociate under the concentrations examined, except below pH 1.

The attainment of equilibrium in the acidic system where $Fe(3,2\text{-opo})^{2+}$ dissociates is quite slow and probably involves undesirable side reactions (see below); thus, a more reliable measure of K_1 is obtained from a quick titration at pH 2.3 in which ligand is titrated into a ferric ion solution (Table XXII). Even in the latter system, though formation of the complex is complete within seconds, there ensues a slow decrease in absorbance over the next few hours.

When dilute solutions of iron and 3,2-Hopo or either 1,2-Hopo ligand were raised above pH 7, a decrease in absorbance occurred over several minutes; upon reacidfication, the absorbance reappeared, albeit slowly. No precipitate was observed, but presumably this decrease in absorbance is due to hydrolysis of the iron (see Discussion). As a practical matter, the slow kinetics of the reverse process means that care must be taken to avoid adding base to the iron(III)–Hopo titration solution.

When solutions several millimolar in 3,2-Hopo (and ca. 2×10^{-5} M Fe^{3+}) were basified above pH 7, instead of precipitation, successive isosbestic processes gave pink solutions of $\lambda_{max} = 494$ and 484 nm, respectively. The first of these isosbestic processes

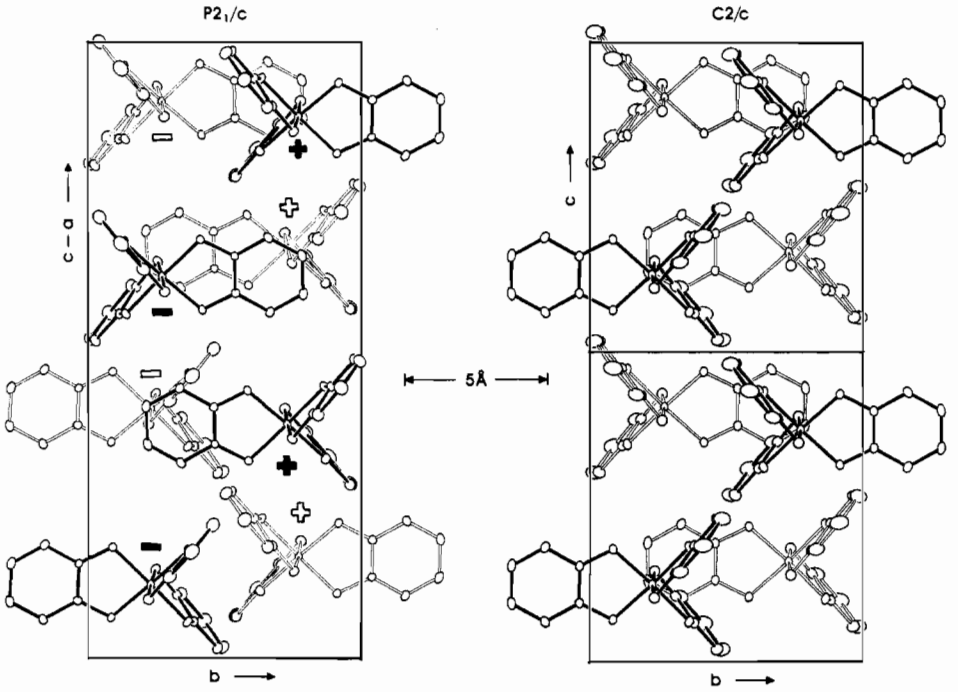

Figure 7. Projection views comparing packing of $Co(1,2\text{-opo})_3$ molecules in **3a** and **3b**. At left is a 101 projection of **3a** and at right a 100 projection of **3b**. Unit cell boundaries are shown. The + and − symbols indicate the Co is ±0.22 Å out of plane; in **3b** all Co atoms are required by symmetry to have $x = 0$ (or $^1/_2$). The molecules with light bonds lie in planes 7.50 (**3a**) and 7.53 (**3b**) Å behind the plane of the dark bonded molecules; in **3a** these are in adjacent unit cells, while in **3b** the light molecules are related to the dark by the *C* center.

corresponds to the monodeprotonation of the tris complex of 3,2-Hopo with iron and has a pK_a of 9.04 that is independent of ligand concentration (at 4 or 17 mM). A second deprotonation occurs around pH 11, although this process may also involve the loss of one of the ligands to form $FeL_2H_{-2}^-$ (where L is 3,2-opo$^-$). This is suggested by the significantly lower pK_{a2} observed for FeL_3 in 4 mM as opposed to 17 mM ligand solution. However, in neither of the high-pH titrations did the data above pH 10 fit well, which suggests other species may be present. Attempts to introduce FeL_3H_{-3} into the solution model did not appreciably improve the fit.

EDTA Competitions. The EDTA–hydroxypyridinone–iron competition experiments were run at pH 4–6 and with sufficient concentration of hydroxypyridinone to ensure the FeL_2–FeL_3 equilibrium would be driven completely to FeL_3. In this pH range the formation of the seven-coordinate $Fe(EDTA)(OH)^{2-}$ species ($pK_a = 7.5$[2]) and the deprotonation of $Fe(Hmim)_3$ (pK_a's = 6.3, 7.4, and 7.4[31]) are of only minor importance, so that inaccuracies in the quoted pK_a's will have minimal effect on the value of K_{eq}.

Table XXIII gives the conditions employed and equilibrium constants obtained for the four hydroxypyridinone ligands investigated by competition with EDTA.

Table XXIII. Conditions and Results of Ligand Competition Experiments Involving EDTA, Hydroxypyridinone Ligand, and Iron(III)[e]

	ligand			
	1,2-Hopo	1,2-Hopo-6-Y	3,2-Hopo	mimosine
temp, °C	25	25	25	25
supporting electrolyte	0.1 M KCl	0.1 M KNO_3	0.1 M $NaClO_4$	0.1 M[a]
no. of experiments	7[b]	12	1	17
C_{Fe}, mM	0.020	0.19–0.38	0.023	0.2–0.4
C_L, mM	0.71–1.14	0.36–1.03	16.9	1.1–5.4
C_{EDTA}, mM	1.02–1.42	0.10–0.40	0.025	0.25–0.5
pH	4.2–5.6	4.0–5.3	5.8	4.4–5.4
K_{eq}[c]	7.3–8.1	15–33		0.17–0.23
K_{eq} (av)	7.4 (4)[d]	25 (6)	9×10^{-6}	0.19 (2)
log K_{eq}	0.88 (2)	1.4 (1)	−5.05	−0.78 (4)
log β_3	26.9 (1)	25.6 (1)	29.6	29.4 (1)

[a] KNO_3, KCl, and $NaClO_4$ were each used for five to six trials. No significant difference in calculated K_{eq} was noted. [b] Three other experiments were not included because of apparent precipitation of $Fe(1,2\text{-opo})_3$. [c] K_{eq} is the equilibrium constant for the reaction $Fe(EDTA)^- + 3Hopo = Fe(opo)_3 + H_2EDTA^{2-} + H^+$. For mimosine, opo$^-$ represents the monoprotonated form, $Hmim^-$. [d] The esd of the last digit is given in parentheses. [e] A value of 25.0 (1) was used for the logarithm of the formation constant for $Fe(EDTA)^-$.[2]

Discussion

The crystal structures of $Co(1,2\text{-opo})_3$, $Fe(1,2\text{-opo})_3$, $Fe(3,2\text{-opo})_3$, and 1,2-Hopo-6-Y consist of discrete molecules with no unusual intermolecular contacts.

The structure of 1,2-Hopo-6-Y is shown in Figure 5. The ring bond lengths show the influence of both resonance forms (localized and aromatic) shown in Figure 1 for 1,2-Hopo. Thus, whereas bonds C3–C4 and C5–C6 are 1.35 Å (about 0.02 Å longer than expected for double bonds), bonds C2–C3 and C4–C5 are ~0.05 Å longer (but still ~0.05 Å shorter than expected for single bonds).

The hydroxyl hydrogen was located in a difference Fourier synthesis and is located so as to hydrogen bond to O2. Both the location of the labile proton (confirming the *N*-hydroxypyridinone rather than a 2-hydroxypyridine *N*-oxide formulation for the predominant tautomer) and the hydrogen bond were predicted by Gardner and Katritzky on spectroscopic grounds.[46] The hydrogen bond is also apparent in the drawing of an otherwise undocumented crystal structure of 5-methoxy-6-methyl-1-hydroxy-2(1*H*)-pyridinone.[47] The bonding to the proton may be considered as an example of unsymmetrical bidentate chelation.

As noted above, the structures of the three metal complexes suffer from disorder. The refined occupancies for the two $Co(1,2\text{-opo})_3$ structures are consistent with an orientational disorder among all trans isomers, a mixture of cis and trans isomers, or all cis isomers. However, a disorder of cis isomers would be expected to give the same nitrogen occupancies (within standard

(46) Gardner, J. N.; Katritzky, A. R. *J. Chem. Soc.* **1957**, 4375–4385.

(47) Itoh, J.; Amano, S.; Ogawa, Y.; Kodama, Y.; Ezaki, N.; Yamada, Y. *J. Antibiot.* **1980**, *33*, 377–382.

deviations) for atoms bound to O12, O21 and O32, which is not observed in structure **3a**. Co(1,2-opo)$_3$ has previously been shown to be low spin; this is consistent with the Co–O distances of 1.88–1.89 Å (vs. 1.895 Å predicted by ionic radii[48]).

The relation between structures **3a** and **3b** are shown in Figure 7. The molecules are approximately cubic close packed in both structures but are elongated perpendicular to the views of Figure 7. The closest Co–Co contacts are within the planes shown; in **3a** there is a 7.37-Å Co–Co distance between molecules of the same chirality and 6.78- and 7.32-Å distances between Λ and Δ isomers. In contrast, both shortest Co–Co distances (6.94 and 7.49 Å) in **3b** are between Λ–Δ pairs.

The room-temperature proton NMR spectrum of Co(1,2-opo)$_3$ (Figure 8), which has been reported previously,[22] contains four analyzable multiplets in the aromatic region. The proton-decoupled ^{13}C NMR spectrum contains only five peaks. These results indicate that in chloroform solution (a) only the cis isomer is present in appreciable quantities (unlikely in light of crystal structure **3a**), (b) only the trans isomer is present, but there are no detectable chemical shift differences between the corresponding positions on the three inequivalent ligands, (c) the cis and trans isomers are both present, but again there are no detectable chemical shift differences, or (d) there is rapid isomerization on the NMR time scale. Alternatives b and c were deemed unlikely, especially since no chemical shift splittings were noticed in the ^{13}C NMR spectrum or in the ^{1}H 300-MHz NMR spectrum at room temperature. However, below 0 °C additional peaks appear in the proton NMR spectra (Figure 8), implicating alternative d.

Although low-spin Co(III) is considered kinetically inert, racemization on the NMR time scale of tris chelate complexes of cobalt(3+) with substituted tropolones has previously been observed.[49] In that study, line-shape analysis indicated a Λ ↔ Δ interconversion proceeding by a trigonal twist mechanism (which causes signals from two of the ligands of the trans isomer to coalesce) and a slower process that results in cis–trans isomerism (which causes complete coalescence to the same number of peaks as in the free ligand). It is not surprising that the hydroxypyridonate complex of Co(III) behaves similarly to the tropolonate complexes in light of the electronic and structural similarities of the two ligands. However, Co(1,2-opo)$_3$ exhibits NMR coalescence approximately 50 °C below that of the tropolone complexes. At the coalescence temperature of ca. 0 °C for Co(1,2-opo)$_3$ the isomerization rate k_I can be estimated from the equation $k_I \approx 2(\Delta\nu)$, where $\Delta\nu$ is the low-temperature chemical shift difference, which in the present case is at least 10 Hz. This is at least 2 orders of magnitude faster than the rate of the cobalt tris(tropolonates).[49,50]

A possible explanation for the rapid isomerization of the 1,2-opo and tropolone complexes of cobalt(III) is thermal accessibility of high-spin cobalt(III) energy levels derived from the $^5T_{2g}$ level of an octahedral field. This explanation was advanced by Taube and co-workers,[51] and more recently by Gray et al.,[52] to account for the relative substitutional lability of low-spin $Co(OH_2)_6^{3+}$. A series of tris(hydroxamate)cobalt(III) complexes has been prepared;[53] some were diamagnetic, while others had magnetic properties intermediate between those expected for singlet and quintet d^6 configurations. We propose that the similar cobalt complexes of 1,2-opo (a cyclic hydroxamate) and tropolones also lie near the low-spin–high-spin crossover.

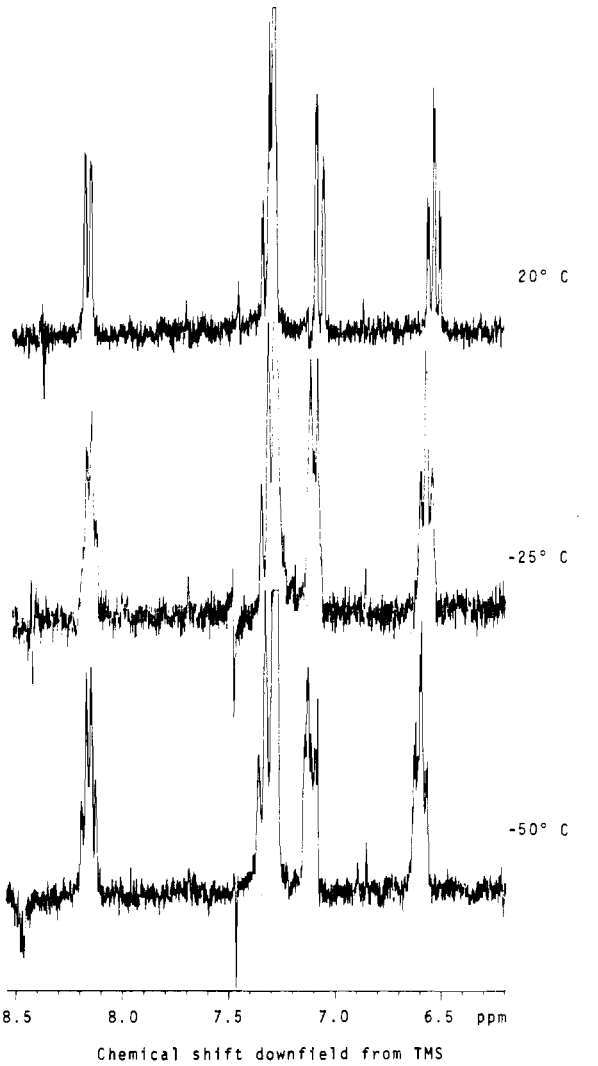

Figure 8. Variable-temperature 250-MHz ^{1}H NMR spectra of Co(1,2-opo)$_3$ in dilute (ca. 1 mM) $CDCl_3$ solution. Chemical shifts are referenced to $CHCl_3$ (δ 7.27). Chemical shifts and J couplings (multiple doublings) at 20 °C (measured in a 10-fold more concentrated solution) are as follows: δ 6.51 (J = 6.9, 6.9, 1.6 Hz, pyr 5-H), 7.04 (J = 1.3 and 8.7 Hz, pyr 3-H), 7.28 (J = 8.7, 7.1, and 1.6 Hz, pyr 4-H), 8.14 (J = 6.7 and 1.3 Hz, pyr 6-H).

Figure 9 shows the approximately hexagonal-close-packed arrangement around one molecule of Fe(3,2-opo)$_3$. Molecules of one stereogeometry (Λ or Δ isomers) are arranged in planes of the hexagonal lattice with Fe–Fe = 9.782 Å. Within these planes there is a 3.30-Å N1–C6 intermolecular contact, which undoubtedly influences the intraplanar packing and is probably responsible for the trigonal twist angle being 5° less than that calculated (Table VIII[54]). The half-occupancy N1···O hydrogen bonds connect enantiomorphic molecules in planes 4.936 Å above and below.

The packing in Fe(1,2-opo)$_3$ is similar, but the lack of hydrogen bonding causes the structure to be axially elongated (interplanar separation 5.212 Å) and compressed within the planes (a = 9.634 Å) relative to Fe(3,2-opo)$_3$. The large (−9°) deviation of the trigonal twist from that calculated for the 1,2-isomer is probably related to the intraplanar compression. Deviations from the ideal D_{3d} twist angle of 60° are much less energetically favorable for low-spin Co^{III} than for high-spin Fe^{III} due to ligand field considerations;[54] this accounts for the different packing arrangement adopted by the cobalt complex. The largest peak in the final difference Fourier map of Fe(3,2-opo)$_3$ (at the origin, 3.56 Å from

(48) Shannon, R. D. *Acta Crystallogr., Sect. A: Cryst. Phys., Diffr., Theor. Gen. Crystallogr.* **1976**, *A32*, 751–767.
(49) Eaton, S. S.; Hutchison, J. R.; Holm, R. H.; Muetterties, E. L. *J. Am. Chem. Soc.* **1972**, *94*, 6411–6426.
(50) Because of the low solubility, small chemical shift differences, and multiple couplings of Co(1,2-opo)$_3$, no attempt was made to analyze line shapes.
(51) Friedman, H. L.; Hunt, J. P.; Plane, R. A.; Taube, H. *J. Am. Chem. Soc.* **1951**, *73*, 4028–4030.
(52) Winkler, J. R.; Rice, S. F.; Gray, H. B. *Comments Inorg. Chem.* **1981**, *1*, 47–51.
(53) Abu-Dari, K.; Barclay, S. J.; Riley, P. E.; Raymond, K. N. *Inorg. Chem.* **1983**, *22*, 3085–3089.
(54) Raymond, K. N.; Isied, S. S.; Brown, L. D.; Fronczek, F. R.; Nibert, J. H. *J. Am. Chem. Soc.* **1976**, *98*, 1767–1774.

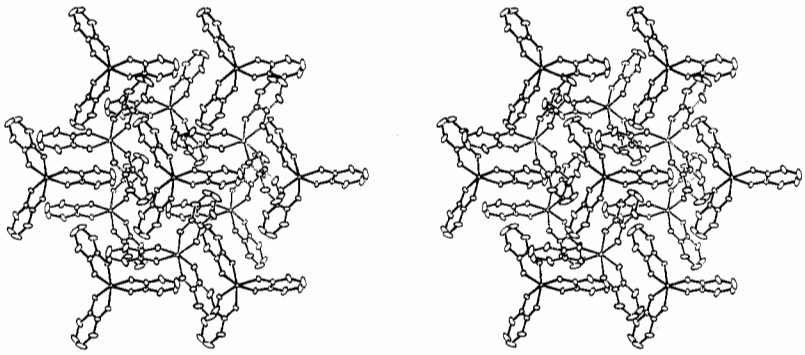

Figure 9. Stereoscopic packing diagram of a molecule of $Fe(3,2\text{-opo})_3$ (**5**) and its 10 nearest neighbors, viewed down the $\bar{3}$ axis of the crystal. For simplicity the positions and 20% probability thermal ellipsoids of the disordered five-atom $R\bar{3}c$ refinement are shown (cf. lower left of Figure 4). The molecules with solid bonds lie in the same plane.

Table XXIV. Average N_1–C_2, C_4–C_5, and (C_3–C_4, C_5–C_6) Bond Lengths (Å) in Various Crystal Structures of 1-Hydroxy-2(1*H*)-pyridinones and Metal Complexes[a]

	N_1–C_2	C_4–C_5	av (C_3–C_4, C_5–C_6)
formal bond order	single	single	double
1,2-Hopo-6-Y	1.383	1.398	1.354
$Th(1,2\text{-opo})_4(OH_2)$[18]	1.364	1.388	1.358
$Th(1,2\text{-opo})_4(MeOH)$[57]	1.35	1.41	1.41
$Co(1,2\text{-opo})_3$ (3a)	1.357	1.380	1.360
$Co(1,2\text{-opo})_3$ (3b)	1.360	1.381	1.352
$Fe(1,2\text{-opo})_3$	1.364	1.400	1.356

[a] Numbering of atoms corresponds to ring position.

Table XXV. Thermodynamic Data Relevant to the Solution Interactions of Ferric Ion with the Four Hydroxypyridinones Studied in This Project and with Catechol and Acetohydroxamic Acid (AHA)[a]

	1,2-Hopo	1,2-Hopo-6-Y	3,2-Hopo	3,4-Hopo	catechol	AHA
$pK_{a,1}$	5.78	5.17	8.66	9.01	13.0	9.36
$pK_{a,2}$	(~0.9)		(0.1)	3.34	9.22	
$\log K_1$	10.3	10.0	11.7	14.2	20.0	11.4
$\log K_2$	9.0	8.5	9.8	11.6	14.7	9.7
$\log K_3$	7.6	7.1	8.1	9.3	9.1	7.2
$\log \beta_3$	26.9	25.6	29.6	35.1	43.8	28.3

[a] The data for the last two ligands come from ref 45 and 2, respectively.

the closest atom (C5), 4.16 Å from H1, and 4.96 Å from the nearest oxygen atom) is attributed to the water of crystallization (indicated by the elemental analysis and apparently lost during collection of the data).

The crystal structures of the tris(hydroxypyridinonato)metal complexes show the expected bidentate coordination through the oxygen atoms. The Fe–O bond distances in the iron(III) complexes are similar to the average distance (2.02 Å) found in tris(catecholato)ferrate(3–) structures[54,55] and are close to the sum of ionic radii of divalent oxygen and high-spin iron(III);[48] $Fe(1,2\text{-opo})_3$,[56] $Fe(1,2\text{-opo-6-Y})_3$, and $Fe(3,2\text{-opo})_3$ are all high spin (variable-temperature magnetic susceptibility). The Co–O distances in both **3a** and **3b** are consistent with low-spin Co(III) (magnetic susceptibility).[22]

The structural disorder complicates interpretation of ligand bond lengths. Table XXIV shows average N_1–C_2, C_4–C_5, and (C_3–C_4, C_5–C_6) bond lengths in the iron, cobalt, and thorium[18,57] complexes of 1,2-Hopo, as well as the corresponding bond lengths in 1,2-Hopo-6-Y. The shortening, by about 0.02 Å, of the N_1–C_2 bond upon complexation is similar to the N–C bond shortening upon hydroxamate complexation[58] and contrasts with the lengthening of the C_1–C_2 bond from 1.38 Å in the diprotonated form[59] to 1.41 Å upon catecholate complexation.[54] These changes suggest increased π-delocalization over the five-membered chelate ring of the hydroxypyridinone and the hydroxamates. The slight changes in the carbon–carbon bond lengths suggest increased delocalization over the entire 1,2-Hopo ring.

The visible spectra of the $Fe(opo)_n^{3-n}$ species are dominated by ligand to metal charge-transfer bands similar to those seen in ferric catecholate and hydroxamate complexes. The intensity of these bands and the use of 10 cm path length cells enabled us to observe the stepwise complexation equilibria spectrophotometrically without the precipitation of the neutral $Fe(opo)_3$ species.

The amide derivative, 1,2-Hopo-6-Y, formed a considerably more soluble ferric complex. This derivative is theoretically capable of binding through the amide oxygen and could plausibly form a six-membered chelate ring reminiscent of the salicylate ligand. The spectra observed in the titrations were virtually identical for the iron–1,2-Hopo and iron–1,2-Hopo-6-Y systems, confirming that the mode of chelation involves the formation of the five-membered chelate ring in both sets of complexes. The same preference for chelation involving only the oxygen atoms attached directly to the (at least partially) aromatic ring has been reported recently for *o*-catechoylamide complexes of Fe(III) and Ga(III).[1,60]

A report on the aqueous solution chemistry of the Fe–3,2-Hopo systems has recently appeared.[61] In acidic solution there is evidence for an oxidation–reduction reaction yielding iron(II) and one-electron oxidized ligand; this is probably responsble for the slow kinetic behavior seen at low pH in our spectrophotometric titrations. These authors report no evidence for a neutral $Fe(3,2\text{-opo})_3$, but they do report a fine purple precipitate in neutral and slightly basic solution containing 3 parts ligand to 1 part iron; this is certainly the tris complex. The observations of these authors are consistent with the formation of charged $FeL_3H_{-2}^{2-}$ or $FeL_2H_{-2}^{-}$ species at high pH, as indicated by our spectrophotometric titrations (Table XXII). The high-pH species may be mixed hydroxypyridinone–hydroxide complexes but may also indicate N-deprotonation of the bound ligands. Such deprotonation has been suggested by Stünzi and co-workers to account for the deprotonation at pH 9–10 of zinc and copper complexes of both 3,2-opo and 3,4-opo.[43]

Slow kinetic behavior resulting in decrease in optical absorbance occurred near neutral pH in all the iron–hydroxypyridinone systems except that of the 3,4-Hopo system. This was always observed after the addition of some base and was originally as-

(55) Anderson, B. F.; Buckingham, D. A.; Robertson, G. B.; Webb, J. *Acta Crystallogr., Sect. B: Struct. Crystallogr. Cryst. Chem.* **1982**, *B38*, 1927–1931.
(56) Landers, A. E.; Phillips, D. J. *Inorg. Chim. Acta* **1981**, *51*, 109–115.
(57) Casellato, U.; Vigato, P. A.; Tamburini, S.; Vidak, M.; Graziani, R. *Inorg. Chim. Acta* **1983**, *69*, 77–82.
(58) Smith, W. L.; Raymond, K. N. *J. Am. Chem. Soc.* **1981**, *103*, 3341–3349.
(59) Brown, C. J. *Acta Crystallogr.* **1966**, *21*, 170–174.
(60) Buckingham, D. A.; Clark, C. R.; Weller, M. G.; Gainsford, G. J. *J. Chem. Soc., Chem. Commun.* **1982**, 779–781.
(61) Howlin, B.; Hider, R. C.; Silver, J. *J. Chem. Soc., Dalton Trans.* **1982**, 1433–1438.

Table XXVI. Tabulation of Formation Constants for the Iron(III)/Mimosine System As Determined by Tsai and Ling[31] and Recast into Conventional Form[h]

reacn	log K	notes
$mim^{2-} + H^+ \rightleftharpoons Hmim^-$	8.76	*a, b*
$Hmim^- + H^+ \rightleftharpoons H_2mim$	7.14	*a, c*
$H_2mim + H^+ \rightleftharpoons H_3mim^+$	2.48	*a, d*
$Fe^{3+} + Hmim^- \rightleftharpoons Fe(Hmim)^{2+}$	12.0	*e, f*
$Fe(Hmim)^{2+} + Hmim^- \rightleftharpoons Fe(Hmim)_2^+$	9.5	*e, f*
$Fe(Hmim)_2^+ + Hmim^- \rightleftharpoons Fe(Hmim)_3$	8.0	*e, f*
$Fe(mim)_3^{3-} + H^+ \rightleftharpoons FeHmim_3^{2-}$	7.42	*a*
$FeHmim_3^{2-} + H^+ \rightleftharpoons FeH_2mim_3^-$	7.43	*a*
$FeH_2mim_3^- + H^+ \rightleftharpoons Fe(Hmim)_3$	6.28	*a*
$Fe^{3+} + 3Hmim^- \rightleftharpoons Fe(Hmim)_3$	29.5	*e, f*
	29.4	*g*

[a] Potentiometric titration. [b] Assigned to hydroxyl group. [c] Assigned to amino group. [d] Assigned to carboxylate. However, there is good evidence that this is in fact the carbonyl protonating and that the pK_a of the carboxylate is ca. 1.1.[43] [e] Spectrophotometric method. [f] Originally reported as constants in which $Hmim^-$ was a hypothetical species protonated only at the amino group with $pK_a = 7.14$. Values have been corrected here so that $Hmim^-$ represents the actual monoprotonated species with $pK_a = 8.76$. [g] This study. [h] Conditions: $T = 25$ °C; $\mu = 0.1$ M; neutral mimosine = H_2mim.

signed to mixed-hydroxide–hydroxamate complex formation. However, a solution model based on the calculated formation constants showed that in all cases where the precipitation had occurred, the solubility product of ferric hydroxide (10^{-38}) had been exceeded and that in cases where no slow kinetic behavior was observed (including the Fe/3,4-Hopo system), the solubility product was not exceeded.

Among the hydroxypyridinones, the stepwise formation constants increase as the oxygen binding groups move away from the ring nitrogen (Table XXV). This is evidence for the importance of the catechol-like resonance form of the iron-bound hydroxypyridinone, since in this aromatic resonance form the nitrogen has a positive charge and will be more stable further from the iron center. The same trend is observed among the pK_a's, although since proton binding is primarily at either the 1- or 3-position of the ring (depending on the isomer), the proton affinity of 3,2-Hopo lies much closer to that of 3,4-Hopo than to that of 1,2-Hopo.

The stepwise formation constants of the Fe–3,4-Hopo system are similar to the constants reported for iron binding by mimosine, an amino acid isolated from the legume *Mimosa paduca*, which contains a 3-hydroxy-4-pyridinone substituent.[31] The protonation

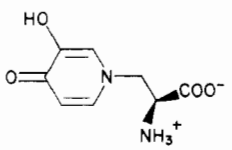

mimosine = H_2mim

of the amino acid grouping complicates the iron complexation equilibria; however, the similarity of the spectra indicate the amino acid grouping is not directly involved in bonding. Table XXVI gives the previously reported formation constants for the Fe/mim system, along with the formation constant of $Fe(Hmim)_3$ determined in this study. The agreement is gratifying.

The stepwise formation constants do not by themselves give much information about a ligand's iron-binding ability, since all high-affinity iron chelators also bind protons at the same sites. This creates a tendency for the ligands to bind iron more effectively at higher pH. However, as the pH increases the ligands must compete with hydroxide for the ferric ion, and this will tend to decrease the ligand's binding effectiveness. Thus most ligands bind iron best in a "pH window" that is not too high and not too low. Figure 10 illustrates the "pH windows" of the hydroxypyridinones of this study as well as other bidentate ligands with high affinities for high-spin ferric ion. The stepwise formation

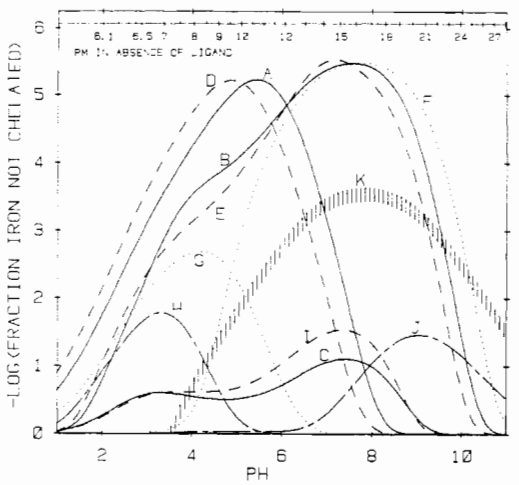

Figure 10. Iron(III)-complexing abilities of various bidentate ligands with high iron affinities. The degree of complexation as a function of pH is plotted as $-\log([Fe']/C_{Fe})$, where [Fe'] is the concentration of uncomplexed iron (including $Fe(OH)_n^{3-n}$ species) and $C_{Fe} = 10^{-6}$ M is the total (analytical) iron concentration in a hypothetical solution assumed to be 10^{-5} M in total ligand.[62] The numbers at the top indicate the pM ($-\log [Fe^{3+}]$) expected in ligand-free 10^{-6} M iron solution as a function of pH (neglecting precipitation of $Fe(OH)_3$). The ordinate may alternatively be interpreted as the increase in pM upon addition of 10^{-5} M ligand. The area under graph K indicates where $Fe(OH)_3$ ($K_{sp} = 10^{-38}$) is expected to precipitate when $C_{Fe} = 10^{-6}$ M. Ligands considered are as follows: (A) 1,2-Hopo; (B) 3,4-Hopo; (C) 3,2-Hopo; (D) *N,N*-dimethyl-1-hydroxy-2(1*H*)-pyridinone-6-carboxamide (1,2-Hopo-6-Y); (E) mimosine; (F) 8-hydroxyquinoline; (G) tropolone; (H) oxalic acid; (I) maltol (3-hydroxy-2-methyl-4-pyrone); (J) catechol. Curves for acetohydroxamic and salicylic acids were also calculated with maxima at pH 3.1 (0.096; 20% complexation) and pH 3.5 (0.22; 40% complexation), respectively.

constants for metal–ligand complexes, ligand-protonation constants, and iron(III) hydrolysis constants[62] were used to compute the fraction of ferric ion bound by a 10^{-5} M ligand solution. The total ferric ion concentration was assumed to be 10^{-6} M. It is assumed that $Fe(OH)_3$ does not precipitate; graph K indicates this assumption is poor for most of the bidentate ligands. However, for $C_{Fe} < 10^{-6}$ M Figure 10 would not substantially change except for graph K, which will decrease with $\log [C_{Fe}]$.

Table XXV and Figure 10 illustrate the interrelatedness of ligand iron and proton affinities. The stepwise formation constants of acetohydroxamate and 3,2-opo with iron(III) are similar, but the greater acidity of 3,2-Hopo makes it a more effective iron chelator under neutral and acidic conditions in which the ligands must deprotonate before binding metals. The acidity of 1,2-Hopo makes it an excellent iron chelator in acidic solution, although its binding ability declines rapidly above pH 6, where the ligand is already completely deprotonated. The "pH window" of 3,4-Hopo binding is shifted to higher pH, making it a better iron chelator near neutral pH. In contrast, catechol, with very large iron *and* proton binding constants, binds iron best in slightly basic solutions.

In addition to the ligands shown in Figure 10, iron binding curves were calculated for other bidentate ligands including amino acids, β-diketonates, salicylic acid, and the low-spin iron chelator *o*-phenanthroline. None of these bound more than 90% of the iron at any pH (for $C_L = 10^{-5}$ M). Hence, it appears that the ligands with the best iron-binding potential have aromatic character and form planar five-membered chelate rings with

(62) Complex formation constants and acid dissociation constants were taken from Tables XXV and XXVI and ref 2. The pK_a's of iron(III) at $T = 25$ °C and $\mu = 0.1$ M were taken to be 2.61,[63] 3.59, 6.8, and 8.9. The last three values were calculated and estimated from information in ref 64.

(63) Sapleszko, R. S.; Patel, R. C.; Matijevic, E. *J. Phys. Chem.* **1977**, *81*, 1061–1068.

(64) Baes, C. F., Jr.; Mesmer, R. E. "The Hydrolysis of Cations"; Wiley: New York, 1976; pp 226–237.

high-spin ferric ion. For acidic solution, 1,2-Hopo and its amide derivative are the most effective bidentate chelators yet investigated, while from pH 7 to 9, 8-hydroxyquinoline, 3,4-Hopo, and mimosine are more effective. Macrochelating ligands containing multiple hydroxypyridinone binding groups should have high affinities for Fe(III) and actinide(IV) ions. The syntheses and properties of these ligands are currently under study.

Acknowledgment. We thank Dr. Fred Hollander of the UC Berkeley CHEXRAY Diffraction Facility (supported in part by the National Science Foundation) for his assistance with various technical aspects of the X-ray diffraction work reported herein and Dr. Vincent Pecoraro for performing the potentiometric titration of 1,2-Hopo. An NSF graduate fellowship to R.C.S. is gratefully acknowledged. This work was supported by NIH Grant HL 24775.

Registry No. **3**, 71560-34-4; **4**, 79649-60-8; **5**, 94781-86-9; **6**, 21190-87-4; **7**, 94781-88-1; **8**, 94781-89-2; **9**, 94781-91-6; **10**, 94781-90-5; **11**, 94781-87-0; Fe(EDTA)$^-$, 15275-07-7; 3,4-Hopo, 1121-23-9; 1,2-Hopo, 822-89-9; 3,2-Hopo, 16867-04-2; $Na_3[Co(NO_2)_6]$, 13600-98-1.

Supplementary Material Available: Tables X-XIX, containing anisotropic thermal parameters, hydrogen atom parameters, and structure factor listings, and Table XXVII, containing IR, NMR, and mass spectral data for compounds **3-11** (61 pages). Ordering information is given on any current masthead page.

Contribution from the Departments of Chemistry, Princeton University, Princeton, New Jersey 08544, and University of California, San Diego, California 92093

Molecular Strain in Chelated-Heme Complexes: Evidence from Resonance Raman Spectroscopy

MELODY L. MITCHELL,† D. H. CAMPBELL,‡ TEDDY G. TRAYLOR,‡ and THOMAS G. SPIRO*†

Received August 28, 1984

Resonance Raman spectra with 406.7-nm laser excitation are reported for chelated heme compounds in which an imidazole is covalently bound to a side chain of mesoheme with linkages of different lengths, and with steric strain introduced by a methyl substituent at the imidazole C2 carbon atom. In the Fe^{III} state, Cl^- and F^- appear to bind in preference to the imidazole, while in the presence of sulfate, a mixture of five-coordinate high-spin (imidazole-bound) and intermediate-spin (sulfate-bound) species is suggested by the Raman spectrum. No conditions were found in which the imidazole and fluoride were bound simultaneously; thus the high-spin six-coordinate F^- complex of heme proteins with proximal imidazole ligands could not be modeled and may have limited intrinsic stability outside the proteins. In the reduced chelated hemes, the imidazole is bound to the iron, and the Fe–Im stretching band is seen at the expected frequency, 204 cm^{-1}. No difference is seen for imidazole linkages of different lengths. In the case of 2-methylimidazole-chelated heme, however, this frequency is markedly decreased, reflecting the steric strain. CO binding was monitored via the upshifted porphyrin skeletal frequencies, as well as the appearance of the Fe–CO stretch near 500 cm^{-1}. This frequency is increased for the 2-methylimidazole-chelated heme, as previously observed for CO adducts with hindered imidazoles. In addition an expansion of the porphyrin core, relative to that of the unhindered chelated hemes, is suggested by a frequency lowering observed for skeletal mode ν_3, which is known to be a core-size marker. This expansion is suggested to be the locus of the force associated with the greater than 10-fold enhancement of the CO dissociation rate in the 2-methylimidazole-chelated heme adduct.

Introduction

The existence of heme proteins with a wide range of ligand-binding properties has inspired efforts to create model compounds with which to test ideas about steric and electronic influences on ligand binding.[1] Chelated hemes (Figure 1) have been synthesized, in which an N-alkylated imidazole ring is anchored to the heme periphery with a chain flexible enough to allow coordination of the imidazole as a fifth ligand to the heme Fe, mimicking the proximal imidazole of hemoglobin.[2] The nature of the chain has been varied to test for steric alterations. For example, the number of methylene groups in the side chain has been reduced from three to two in order to strain (i.e. tilt) the iron–imidazole linkage. Another modification involves methylating the imidazole C2 atom, to hinder the Fe atom from moving into the heme plane. Effects of these and other modifications on the CO- and O_2-binding kinetics have been evaluated.[2-4]

Resonance Raman (RR) spectroscopy provides a probe of heme structure.[5] Laser excitation within the porphyrin π–π^* transitions in the visible and in the ultraviolet region provide selective excitation of porphyrin vibrational modes, which are sensitive to structural effects induced by alterations in the state of the central Fe atom and its axial ligands. The technique is equally applicable to heme proteins and to heme model compounds in solution. In this study we examine structural variations in chelated hemes using resonance Raman spectroscopy. In the Fe^{III} state, high-spin adducts have been found to be five-coordinate; there appears to be little propensity to form six-coordinate analogues of metmyoglobin. In the Fe^{II} state, the Fe–imidazole bond strength is apparently unaffected by shortening of the imidazole linkage but is significantly weakened by the introduction of a C2 methyl group on the imidazole. In the CO adduct the steric strain appears to be accommodated by an expansion of the porphyrin core.

Experimental Section

Mesohemin mono-3-(1-imidazolyl)propylamide monomethyl ester (**1**) (see Figure 1), mesohemin mono-2-(1-imidazolyl)ethylamide monomethyl ester (**2**), and mesohemin mono-3-(2-methyl-1-imidazolyl)-propylamide monomethyl ester (**3**) were prepared as mixtures of five-coordinate chelated-imidazole or chloride-bound species.[3,6]

Ferric Porphyrins. Conversion of **1** to a single species was accomplished by dissolving 1 mg in 5 mL of CH_2Cl_2 (reagent grade) and washing three times with equal volumes of 5% Na_2CO_3 to form the μ-oxo dimer. The olive green solution was then washed twice with equal volumes of NaCl/HCl (0.25/0.01 M), NaF/HF (0.25/0.01 M), or 0.01 N H_2SO_4. Absorption spectra for each species are reported in Figure 2. The acid is necessary to cleave the μ-oxo dimer. When the 0.01 N H_2SO_4 washed species was subsequently washed with 50 mM NaF or NaCl, the

† Princeton University.
‡ University of California.

(1) Collman, J. P.; Halbert, T. R.; Suslick, K. S. In "Metal Ion activation of Dioxygen"; Spiro, T. G., Ed.; Wiley-Interscience: New York, 1980; pp 1-72.
(2) Traylor, T. G.; Chang, C. K.; Geibel, J.; Berzinis, A.; Mincey, T.; Cannon, J. *J. Am. Chem. Soc.* **1979**, *101*, 6716.
(3) Geibel, J.; Cannon, J.; Campbell, D.; Traylor, T. G. *J. Am. Chem. Soc.* **1978**, *100*, 3575.
(4) Traylor, T. G.; Campbell, D.; Sharma, V.; Geibel, J. *J. Am. Chem. Soc.* **1979**, *101*, 5376.
(5) Spiro, T. G. In "Iron Porphyrins"; Lever, A. B. P., Gray, H. B., Eds.; Addison-Wesley: Reading, MA, 1983; Part II, pp 89-160.
(6) Chang, C. K.; Traylor, T. G. *J. Am. Chem. Soc.* **1973**, *95*, 8475.

0020-1669/85/1324-0967$01.50/0